Moonlighting α-PheRS connects JAK/STAT with Notch signaling for intestinal homeostasis

Manh Tin Ho[1], Jiongming Lu[2], Beat Suter[1]

Affiliations:

[1]Institute of Cell Biology, University of Bern, Baltzerstrasse 4, Bern 3012, Switzerland.

[2]Present address: Max Planck Institute for Biology of Ageing, 50931 Köln, Germany.

Corresponding author: beat.suter@izb.unibe.ch

Running title: Proliferation and homeostasis function of α-PheRS

Keywords: aminoacyl tRNA synthetase, Notch signaling, JAK/STAT signaling, stem cell, differentiation, proliferation, intestinal tumor, Drosophila

Abstract

Phenylalanyl tRNA synthetase (PheRS) levels are elevated in multiple cancers and, interestingly, also in normal stem cells. Our results show that elevated levels of the *α-PheRS* subunit stimulate cell proliferation in different tissues, while downregulation of *α-PheRS* reduces organ size. Furthermore, overexpression of *α-PheRS* in stem- and progenitor cells caused over-proliferation in the intestine, a phenotype indistinguishable from the *Notch* RNAi phenotype in the same cells. Importantly, the phenotype caused by high levels of α-PheRS can be rescued by simultaneously overexpressing Notch, suggesting that *α-PheRS* induces this phenotype by downregulating *Notch*. High levels of α-PheRS in neuroblasts also cause the same phenotype as knocking down *Notch* in these cells, even though Notch signaling in the neuroblast lineage serves an opposite function by promoting neuroblast proliferation and maintenance. α-PheRS might, therefore, act as a general novel regulator of Notch signaling. α-PheRS levels, in turn, are controlled by Stat92E, the transcription factor of the JAK/STAT signaling pathway that is needed for the differentiation of intestinal stem cells during normal tissue homeostasis. From this, we conclude that the α-PheRS subunit can transmit the activity status of the JAK/STAT pathway to the Notch pathway as a mechanism to coordinate stem cell proliferation with differentiation. In this process, α-PheRS levels balance between tissue development and tissue growth to regulate tissue homeostasis. For its established essential function as an aminoacyl tRNA synthetase, α-PheRS needs to bind to β-PheRS in every cell to form the $\alpha_2\beta_2$ heterotetramer that loads the amino acid phenylalanine onto the cognate $tRNA^{Phe}$. Here we also demonstrate that the newly identified activities of α-PheRS are moonlighting functions, independent of the aminoacylation activity of PheRS, and they do not visibly stimulate translation.

Introduction

Many cancer tissues display higher levels of Phenylalanyl-tRNA synthetase (PheRS, FARS or FRS) than their healthy counterparts according to the database "Gene Expression across Normal and Tumor tissue" (GENT2; published 11 July 2019). Interestingly, a correlation between tumorigenic events and PheRS expression levels had been noted already much earlier for the development of myeloid leukemia (Sen et al., 1997). Despite this, a possible causative connection between elevated PheRS levels and tumor formation had so far not been reported and, to our knowledge, also not been studied. This might have been due to the assumption that higher PheRS levels could simply reflect the demand of tumorigenic cells for higher levels of translation, or it could have to do with the difficulty of studying the moonlighting function of a protein that is essential in every cell for basic cellular functions such as translation.

Aminoacyl-tRNA synthetases (aaRSs) are important enzymes that act by charging transfer RNAs (tRNAs) with their cognate amino acid, a key process for protein translation. This activity makes them essential for accurately translating the genetic information into a polypeptide chain (Schimmel and Soll, 1979). Besides their well-known role in translation, an increasing number of aaRSs have been found to perform additional functions in the cytoplasm, the nucleus and even outside of the cell (Guo and Schimmel, 2013; Nathanson and Deutscher, 2000; Smirnova et al., 2012) (Casas-Tinto et al., 2015; Gomard-Mennesson et al., 2007; Greenberg et al., 2008; Otani et al., 2002; Zhou et al., 2014). Moonlighting aaRSs regulate alternative splicing, RNA processing and angiogenesis (Lee et al., 2004). For example, the amino-acid binding site of LysRS has an immune response activity; or TrpRS inhibits the vascular endothelial (VE)-cadherin, which elicits an anti-angiogenesis activity (Tzima et al., 2005; Yannay-Cohen et al., 2009).

Cytoplasmic PheRS is one of the most complex members of the aaRSs family, a heterotetrameric protein consisting of 2 alpha- (α) and 2 beta (β)-subunits responsible for charging $tRNA^{Phe}$ during translation (Roy and Ibba, 2006). The α subunit includes the catalytic core of the tRNA synthetase and the β subunit has structural modules with a wide range of functions, including tRNA anticodon binding, hydrolyzing mis-activated amino acids, and editing misaminoacylated $tRNA^{Phe}$ species (Ling et al., 2007; Lu et al., 2014; Roy and Ibba, 2006). Precision of the initial charging reaction and proper editing are both important for the cell and the organism because mutations in the amino-acid recognition and editing sites of Drosophila *PheRS* cause sieving defects that lead to mis-incorporation of amino acids into proteins, ER stress, apoptosis, shortened life span, as well as neural degeneration (Lu et al., 2014).

We set out to address the question whether and how elevated levels of PheRS can contribute to tumor formation. To test for this activity, we studied the role of PheRS levels in the Drosophila model system with the goal of dissecting the molecular mechanism of such a moonlighting role of *PheRS*. We found that α-PheRS levels regulate cell proliferation, cell differentiation or both in different tissues and cell types. We now show that elevated levels of α-PheRS do not simply act to allow higher levels of translation, but control signaling mechanisms involved in differentiation and proliferation control. Although the consequences of altered levels vary to some degree between tissues, we found that even in two tissues with the most divergent consequences, PheRS levels acted by repressing the Notch signaling pathway, suggesting that this regulative mechanism is responsible for all moonlighting activities of α-PheRS described here. α-PheRS levels, in turn, are controlled by JAK/STAT signaling in the intestinal system, placing α-PheRS at the intersection between two signaling pathways for the fine tuning of normal tissue homeostasis in the midgut. Focusing on the intestine and intestinal stem cells revealed that elevated α-PheRS levels are tumorigenic in the

intestinal model. Given the high demand for research on intestinal diseases and cancer (Markowitz and Bertagnolli, 2009) our work now opens new avenues to test ways to control tissue homeostasis and tumor formation.

Results

A non-canonical α-PheRS activity is sufficient to induce additional M-phase cells

To test whether elevated levels of PheRS can stimulate growth or proliferation when other aaRSs are not overexpressed, we overexpressed α-PheRS, β-PheRS, and both subunits together in the posterior compartment (P) of wing discs using the *engrailed-Gal4* (*en-Gal4*) driver. In this assay the anterior compartment expresses normal endogenous levels and serves as an internal control. When α-PheRS was overexpressed in the posterior compartment either alone or together with β-PheRS, the mitotic marker phospho-histone H3 (PH3) revealed a 40% increase in mitotic cells in the posterior (P) compartment relative to the anterior (A) one of the same disc (Fig 1A-C). Because elevated levels of the α-PheRS subunit alone are sufficient for the increase in mitotic cells, this effect is unlikely caused by increased $tRNA^{Phe}$ aminoacylation activity and translational activity, which requires both subunits.

To test this interpretation, we made a mutant version of α-PheRS in which Tyr412 and Phe438 are replaced by Cysteins. These substitutions are predicted to block the entrance into the phenylalanine binding pocket, preventing binding of Phe and aminoacylation of $tRNA^{Phe}$ by the mutant $PheRS^{Cys}$ (Finarov et al., 2010). To test whether the $PheRS^{Cys}$ substitution indeed reduces the aminoacylation activity of PheRS, we expressed mutant and wild-type α-PheRS subunits together with β-PheRS subunits in E. coli, purified them and performed aminoacylation assays. As opposed to the strong enzymatic activity of the wild-type α-PheRS plus β-PheRS subunits, the $\alpha\text{-}PheRS^{Cys}$ together with wild-type β-PheRS produced only the same background signal as the α-PheRS subunit alone (Supplementary Fig S1). The same mutations were also introduced into a genomic clone and the resulting transgenic $\alpha\text{-}PheRS^{Cys}$ was not able to rescue the $\alpha\text{-}PheRS^{G2060}$ mutant, indicating that the Cys mutant is indeed not

functional in aminoacylation in vivo in Drosophila. Overexpressing a transgenic *α-PheRS*^{Cys} in the posterior compartment of the wing disc also caused a 67% increase in the number of mitotic cells in the above assay (Fig 1C). The fact the mutant *α-PheRS*^{Cys} version caused an increase in mitotic cells at least as strongly as the wild-type *α-PheRS,* together with the fact that β-PheRS overexpression was not needed for this effect, clearly demonstrates that the canonical function of *PheRS* is not required to cause the elevated frequency of mitotic cells.

We also tested directly whether PheRS overexpression is unable to cause elevated translation as we expected. For this, we analyzed general protein synthesis activity in the two wing compartments by puromycin staining using the ribopuromycylation method (RPM) (Deliu et al., 2017). Overexpression of the transcription factor dMyc increases protein synthesis activity and was therefore used as a positive control for detection of elevated translation and PMY labeling (Deliu et al., 2017). Indeed, when comparing signal intensity in the posterior compartment to the intensity in the anterior compartment of the same disc, dMyc overexpression significantly increased the anti-PMY signal in the expressing posterior compartment. In contrast, neither overexpression of α-PheRS alone nor combined with β-PheRS increased the puromycin labeling in the overexpressing compartment (Fig 1D-E'', F). The combined results therefore demonstrate unambiguously that elevated α-PheRS levels cause additional cells to be in mitosis through an aminoacylation- and translation-independent, non-canonical activity. α-PheRS levels might specifically slow down progression through M-phase, causing higher numbers of cells to remain in the PH3-positive state. Alternatively, they might either promote over-proliferation of mitotic cells or induce proliferation in non-cycling cells.

High α-PheRS tolerance in an organ with tight size control

To find out whether the increased number of mitotic cells in the region expressing higher α-PheRS levels leads to a different compartment size, we measured the size of two clearly defined regions in the posterior (P) and the anterior (A) compartment of the adult wing as shown in Fig 2A. Normalizing the size of the posterior region (P) to the size of the anterior region (A), we calculated the P/A ratio (Fig 2B). Even though α-PheRS alone was sufficient to induce additional mitotic cells in larval discs, this did not cause the formation of a larger wing in the adult. Co-overexpression of both subunits was needed to cause a small, but significant increase of the posterior region of the wing (Fig 2B). This size increase does not appear to be a general property of elevated aaRS levels because overexpression of Glycyl-tRNA synthetase (GlyRS; (Niehues et al., 2015)) with the same driver did not increase wing size (Fig 2B). The final size of this particular organ is tightly controlled by different mechanisms that are only partially understood, but are capable of compensating for differences in growth and proliferation such that the compartments reach their correct final size even if they grew at different rates at an earlier stage (Hariharan, 2015; Martin and Morata, 2006). To better understand the consequences of high PheRS levels in the discs, we studied its effect on dissociated cells and found that elevated PheRS levels primarily affected cell size, whereas proliferation remained controlled or was compensated for (Supplementary data, Fig S2A,B).

We considered the possibility that PheRS might signal availability of Phe to TORC1, which links cell growth to amino acid availability (Laplante and Sabatini, 2012; Wullschleger et al., 2006). Such a mechanism would be analogous to the function of LeuRS in this pathway (Bonfils et al., 2012; Han et al., 2012). However, experimental testing of this hypothesis did not uncover any evidence for such a signaling function (Supplementary data, Fig S3A,B).

The *α-PheRS* subunit accelerates proliferation in different tissues and its knockdown reduces organ size

To test the effects of PheRS levels on proliferation directly and in a different organ and cell type, we set up a mosaic analysis with repressible cell marker (MARCM; (Wu and Luo, 2006) assay in the follicle cells. Twin spot clones were generated with one clone overexpressing PheRS and the GFP marker, and its twin clone expressing normal endogenous levels of PheRS and serving as an internal control (Fig 3A). The results of this experiment showed that clonal overexpression of both subunits of PheRS accelerated the proliferation of the overexpressing cells on average by 32% (Fig 3B). Overexpression of GFP with only the β-PheRS subunit or with GlyRS did not significantly promote clonal expansion (Fig 3B), confirming that the activity of stimulating growth and proliferation is specific for PheRS and not a general role of aaRSs. Interestingly, overexpression of GFP with the α-PheRS subunit alone also stimulated cell proliferation autonomously by 30% (Fig 3B) and, intriguingly, this was very close to the 32% increase calculated for the clone overexpressing both PheRS subunits (Fig 3B). Remarkably, the higher number of mitotic cells observed upon α-PheRS overexpression in the posterior compartment of the larval wing discs (Fig 1C) was in a comparable range as the proliferation increase in the follicle cell assay (Fig 3B). These results therefore show that α-PheRS levels promote cell proliferation and they suggest that it has this activity in different tissues.

Overexpression of *α-PheRS*^{Cys} alone and *α-PheRS*^{Cys} together with *β-PheRS (PheRS*^{Cys}) stimulated clonal growth and cell proliferation in the follicle cell twin spot experiment by 28% and 25%, respectively (Fig 3B), again confirming that this is an aminoacylation-independent activity. It is tempting to speculate that the slightly lower increase in proliferation upon

overexpressing the mutant *α-PheRS*^{Cys} (28%) in twin spot clones compared to wild-type *α-PheRS* (30%) could be due to reduced translation caused by the overexpression of an inactive α subunit that is predicted to partially act as a dominant negative subunit for the aminoacylation function. If this proliferation function is important for development and homeostasis, reduced *α-PheRS* activity should lead to problems in these processes. Because *α-PheRS* and *β-PheRS* are both essential genes in Drosophila (Lu et al., 2014), we used RNAi to reduce their activity in specific tissues by RNAi (Fig S4A,B). Indeed, knock down in the developing eye reduced the adult eye, whereas knockdown in the larval fat body reduced the size of the entire pupae. Furthermore, RNAi knockdown *α-PheRS* or *β-PheRS* in Kc cells caused these cells to proliferate more slowly than the control cells (Fig S4C). Although it is not clear from these results, which activity of PheRS causes this effect, the phenotypes observed are consistent with a direct function in regulating proliferation.

α-PheRS promotes stem cell proliferation in the midgut and high expression leads to hyper- and dysplasia

Tissue growth and homeostasis play important roles in developing and outgrown animals, and they require tight control of stem cell self-renewal and differentiation of daughter cells. The Drosophila midgut is a powerful model to analyze these mechanisms and their interplay. Intestinal stem cells (ISCs), also referred to as adult midgut progenitors (AMPs) in the larval gut, can either divide asymmetrically or symmetrically. After an asymmetric division, one daughter cell differentiates into an absorptive enterocyte (EC) or a secretory enteroendocrine (EE) cell, the other keeps its stem cell identity (Micchelli and Perrimon, 2006; Ohlstein and Spradling, 2007). We investigated the effect of overexpression of each PheRS subunit in larval ISCs by using the *esg-Gal4* driver, which expresses specifically in ISCs. Co-expression of

222 *UAS-YFP* allowed us to monitor the *esg-Gal4* activity. The results demonstrated that
223 overexpression of Myc::α-PheRS alone in the larval midgut caused the numbers of YFP
224 positive ISC cell clusters in the posterior midgut to increase. In addition, the number of YFP
225 positive cells per cluster increased as well (Fig 4A, B, D-D'). The increase of both numbers
226 was significant when compared to posterior midguts expressing normal levels of α-PheRS (Fig
227 4A, B, C-C'). Overexpression of β-PheRS::V5 alone did not produce such a phenotype (Fig
228 4A, B, E-E'). Interestingly, when both PheRS subunits were overexpressed, the guts also
229 showed an increase in the number of YFP positive ISC clusters. However, the increase was
230 less pronounced and the number of YFP positive cells per cluster remained unchanged (Fig
231 4A, B, F-F').

232 Driving the expression of the α-PheRS^{Cys} mutant alone in ISCs also produced
233 additional ISCs, indicating again that the aminoacylation function is not required for this
234 activity (Fig 4G). Surprisingly, however, this treatment induced the over-proliferative
235 phenotype in both anterior and posterior areas of the larval midgut (outlined with white dashed
236 lines, Fig 4G, G') while the overexpression of wild-type Myc::α-PheRS gave rise to high
237 numbers of ISCs only in the posterior midgut (Fig 4D, D'). Interestingly, elevated α-PheRS^{Cys}
238 levels also caused the appearance of a more severe, tumor-like phenotype, where individual
239 ISC clusters could not be discerned anymore. Furthermore, instead of the wild-type gut
240 phenotype, characterized by a majority of ECs with large nuclei, interspersed with occasional
241 ISC clusters with smaller nuclei (as seen in the YFP overexpression control, Fig 4C, C'), we
242 observed a phenotype where ECs and ISCs could not be distinguished based on the size of their
243 nuclei, but emerged as a larger cell population with intermediate size nuclei (Fig 4G'). Many
244 of these cells expressed the *esg*>YFP stem cell marker at high levels, but others displayed only
245 a very weak YFP signal. One possible interpretation of this phenotype could be that α-PheRS^{Cys}
246 overexpressing ISCs progress through the cell cycle more rapidly such that they are not able to

grow to their proper size and do not have sufficient time to turn over the YFP. Staining these guts for the mitotic marker PH3 demonstrated that the posterior midgut contained clearly more and a higher proportion of PH3 positive cells. Significantly, more cells were labelled by anti PH3 staining in the posterior midgut when α-PheRS or the α-PheRS^{Cys} mutant were overexpressed alone in ISCs (Fig 4H, I). Again, this suggests that cells in these areas display an elevated proliferation rate.

In a normal adult midgut, ISCs are found as characteristic single cells or as pairs with their daughter enteroblast (EB). Both cell types are labeled with YFP when their expression is driven by *esg*-Gal4 (Fig 4J). Overexpression of only α-PheRS or α-PheRS^{Cys} in these adult ISCs caused a strong phenotype, too. It induced hyperplasia and dysplasia in regions R4-R5 of the posterior midgut. Similar to the hyperplasia phenotype observed in the larval gut, we observed cells adjacent to ISC clusters displaying the YFP stem cell marker, even though they contained large nuclei (Fig 4J'-J"), indicative of a dysplasia phenotype. We conclude that in the larval and adult guts, elevated α-PheRS expression can elevate the proliferation rate of stem cells and lead to hyper- and dysplasia.

Elevated α-PheRS levels prevent proper differentiation and gut homeostasis by downregulating Notch signaling

Asymmetric divisions of ISCs give rise to a new ISC and an undifferentiated EB. Differential Delta/Notch signaling between the new ISC and the EB causes the latter to either differentiate into an absorptive EC or a secretory EE (Micchelli and Perrimon, 2006; Ohlstein and Spradling, 2007). To investigate how α-PheRS affects the fate decision in this lineage, we studied the cell population in the posterior midgut. In larval and adult guts, the over-proliferation phenotype caused by α-PheRS^{Cys} overexpression showed a significantly elevated ratio between EEs and

ECs (Fig 5A-A', B-B', C). The overexpression of *α-PheRS* alone with the *esg-Gal4* driver caused the same changes, albeit with a slightly lower expressivity (Fig 5C). These observations indicate that overexpression of α-PheRS or α-PheRS^{Cys} directs EB differentiation to the EE fate and interferes with EC differentiation.

Differentiating ISC daughter cells, EBs, adopt the EE fate when their *Notch* activity is low and the EC fate if their *Notch* activity is high (Takashima et al., 2011). Furthermore, because *Notch* activity is needed for EB differentiation, reduced *Notch* activity leads to EE-like and ISC-like tumors (Micchelli and Perrimon, 2006; Patel et al., 2015; Wang et al., 2015; Yin and Xi, 2018). Indeed, in regions where the normal cellular composition of the larval gut was transformed, we observed an increase in the number of cells and in particular a cell population with intermediate size nuclei upon RNAi treatment of *Notch* with the *esg-Gal4* driver (white dashed line, Fig 5D-D'). The similarity between the two phenotypes suggests that overexpression of *α-PheRS* or *α-PheRS^{Cys}* might cause this phenotype by reducing *Notch* activity. Indeed, as seen in Fig 5F, overexpression of *α-PheRS* and *α-PheRS^{Cys}* downregulates the *Notch* activity reporter NRE-EGFP (Notch response element promoter driving the expression of eGFP; (Housden et al., 2012) and overexpressing *Notch* together with *α-PheRS^{Cys}* in the same midgut ISCs rescued the tumor-like midgut phenotype, giving rise to midguts with a wild-type appearance (Fig 5A", B", E-E'). This shows that α-PheRS levels control *Notch* activity and that high α-PheRS levels cause the tumor-like phenotype in the midgut by downregulating *Notch* activity.

α-PheRS is a novel general repressor of Notch signaling

Developing larval brains contain neuroblast (NB) stem cells that divide asymmetrically to either keep the stemness and or to differentiate into neuronal cells. *Notch* signaling plays a

crucial role in this process (Ables et al., 2011; Giachino and Taylor, 2014), but in contrast to the situation in the gut, loss of *Notch* prevents NB self-renewal, and ectopic expression of *Notch* leads to tumor formation (de la Pompa et al., 1997; Grandbarbe et al., 2003; Hatakeyama et al., 2004). This opposite role of *Notch* makes the NB lineage an ideal complementary system to test whether α-PheRS is a general component of the *Notch* pathway. Driving α-PheRS or the α-PheRS^{Cys} expression in NBs with the *inscutable-Gal4 (incs-Gal4)* driver resulted in significantly smaller central brains (CB), the region where the NBs are located (Fig 6A-A'', B). In contrast, this treatment had little or no effect on the size of the optic lobes (OL). The phenotype was indistinguishable from the phenotype caused by *Notch* knock-down (Fig 6B), and co-overexpression of Notch with α-PheRS^{Cys} in neuroblasts rescued the brains to wild-type size (Fig 6B).

Type II neuroblasts are particularly suited to analyze effects on neuroblast differentiation. Targeting specifically the 8 type II neuroblasts in central brain lobes with *α-PheRS* or *α-PheRS^{Cys,}* overexpression, resulted in half of the central brains in a strong reduction of the number of neuroblasts, and the resulting central brain lobes ended up smaller (Fig 6C and Supplementary Fig S5). Knocking down *Notch* in type II NBs with RNAi and the same driver combination resulted in a similar phenotype, but with a higher expressivity. On the other hand, overexpression of Notch in α-PheRS overexpressing type II neuroblasts partially rescued the number of type II neuroblasts to wild-type numbers and it restored the normal size of the brain (Fig 6C and Supplementary Fig S5). Because the effect on Notch signaling is the same in guts and brains, two tissues where *Notch* has opposing functions on cellular differentiation, we conclude that *α-PheRS* is a novel general repressor of Notch signaling.

Transcription factor Stat92E of the JAK/STAT pathway regulates α-PheRS levels

Under normal conditions, the JAK/STAT signaling pathway induces progenitor differentiation into ECs via regulating Notch activity (Herrera and Bach, 2019). Under stress conditions like bacterial infection, secreted Unpaired3 (Upd3) acts as a cytokine that activates JAK/STAT signaling, leading to ISC proliferation and differentiation to repair the damaged parts of the gut (Buchon et al., 2009; Lin et al., 2010). Upd3 not only activates JAK/STAT signaling, but also *Notch* activity to enhance ISC proliferation and to promote EC differentiation, respectively (Jiang et al., 2009). Because α-PheRS levels affect Notch signaling, too, we therefore tested whether α-PheRS could possibly coordinate JAK/STAT with Notch signaling. The *Stat92E* gene encodes the transcription factor at the downstream end of the JAK/STAT pathway. Using the hypomorphic $Stat92E^{HJ}$ allele, we tested whether suppressing JAK/STAT signaling affects α-PheRS expression. Indeed, $Stat92E^{HJ}$ mutants displayed elevated levels of α-PheRS in Delta-positive ISC cells (Fig 7A-B"). Consistent with this result, *Stat92E* knock-down by RNAi with the *esg-Gal4* driver also showed elevated α-PheRS levels in ISC cells (Fig7C-C"). As shown in Fig 7 D-D', E-E', F-F', G, the levels of α-PheRS significantly increased in ISCs/EBs. The fact that two different approaches to reduce *Stat92E* activity lead to higher α-PheRS levels in ISCs/EBs clearly demonstrates that *Stat92E* regulates α-PheRS levels in these cells.

Surprisingly, RNAi knock down of *Stat92E* with the *esg-Gal4* driver not only affected α-PheRS levels in ISCs, but also in some neighboring polyploid ECs, but not in distant ECs (arrows in Fig7C", F) (Fig7G). Because we also observed this phenotype in $Stat92E^{HJ}$ mutants (arrows in Fig 7E) (Fig 7G), this is unlikely to be an off-target effect of the RNAi. It thus appears that *Stat92E* can normally control α-PheRS levels also in a cell non-autonomous way. To test if *Stat92E* is not only required for downregulation of α-PheRS, but also sufficient, we overexpressed *Stat92E* in ISCs and EBs. Indeed, elevated-Stat92E levels reduced the α-PheRS signal in ISCs and EBs (Fig 7H-I"). On the other hand, high levels of α-PheRS did not affect

343 *Stat92E* activity when assayed with the *10X STAT92E-GFP* reporter (Bach et al., 2007) (Fig
344 7J-K"'). We conclude that *Stat92E* can regulate α-PheRS levels specifically in EBs and ISCs
345 to maintain stem cell homeostasis. Together with the result that α-PheRS regulates Notch
346 signaling, we therefore identified α-PheRS as an intermediate factor that links the JAK/STAT
347 pathway to Notch signaling to regulate gut homeostasis.

348

Discussion

Our work revealed that *PheRS* not only charges tRNAs with their cognate amino acid Phe, but that it also performs moonlighting functions in regulating cell proliferation and differentiation in different tissues. Levels of α-PheRS are critical for these regulative processes and these levels are generally elevated in healthy stem cells compared to differentiated cells. Similarly, many tumor cells show elevated α-PheRS levels compared to their healthy counterparts and a positive correlation between these levels and tumorigenic events had been noted quite some time ago (Sen et al., 1997). Several circumstantial and direct evidence show that elevated α-PheRS levels do not simply allow higher translational activity to overcome a growth rate restriction imposed by hypothetically limiting levels of PheRS. In fact, PheRS is unlikely to be rate-limiting for cellular growth. because animals with only one copy of the *α-PheRS* or *β-PheRS* gene do not show a phenotype (Lu et al., 2014) and tissue culture cells can be stimulated to grow more rapidly without stimulating the expression of the two PheRS genes (Chen et al., 2003) (Lu et al., 2014). Indeed, directly measuring translational activity *in situ* (Fig 1D-D") showed the same levels of translation whether *α-PheRS* was overexpressed or not. Furthermore, aminoacylation of $tRNA^{Phe}$ requires the tetrameric protein $\alpha_2\beta_2$-*PheRS*. However, overexpression of an aminoacylation-dead *α-PheRS*^{Cys} mutant subunit alone, (without simultaneous overexpression of the β-PheRS subunit) already lead to the accumulation of numerous additional dividing cells, closely resembling the phenotype observed when the wild-type gene was expressed in the same way. We therefore conclude that this activity of *α-PheRS* is independent of the translational function of *PheRS*.

The notion that the α-PheRS subunit can be stable and it functions independently of the β-subunit was surprising because previous results showed that the two subunits were dependent on the presence of the other subunit for their stability (Antonellis et al., 2018; Lu et al., 2014).

Our results now show that this requirement does not apply to all cell types. In young follicle cells, ISCs and possibly other dividing cells, the overexpression of the α-PheRS subunit alone results in higher levels of α-PheRS accumulation and, in particular when elevated levels were induced in gut ISCs and EBs, this produced a strong phenotype. This suggests that the α- and β-PheRS subunits function together in every cell to aminoacylate $tRNA^{Phe}$, but in addition, the α-subunit can be stable in specific cell types, such as stem cells, where it assumed a novel function in regulating cell proliferation and differentiation.

PheRS is not the only aaRS family member for which roles beyond charging tRNAs have been identified (Dolde et al., 2014). For instance, MetRS/MRS is capable of stimulating the rRNA synthesis (Ko et al., 2000), GlnRS/QRS can block the kinase activity of apoptosis signal-regulating kinase 1 (ASK1) (Ko et al., 2001) and a proteolytically processed form of YARS/TyrRS acts as a cytokine (Casas-Tinto et al., 2015; Greenberg et al., 2008). aaRSs are, however, also not the only protein family which evolved to carry out more than one function. In recent years it has become increasingly evident that many if not most proteins have evolved to carry out not only one, but two or more functions, providing interesting challenges to figure out, which of their activities are important for the individual functions of a protein (Dolde et al., 2014).

We found that elevated levels of α-PheRS promote cell proliferation in different cell types. In follicle cells, more cells were produced in the α-PheRS overexpressing clones compared to wild-type clones. In wing disc, more mitotic cells were detected in the α-PheRS overexpressing compartments. In the gut tissue, elevated $\alpha\text{-PheRS}^{(Cys)}$ levels produced 2-5 times as many cells with intermediate size nuclei that stained positive for stem cell markers. Similarly, these guts also contained 5-8 times as many mitotic cells when $\alpha\text{-PheRS}^{(Cys)}$ was overexpressed. Together, these results strongly suggest, that also in this situation the higher

levels of α-PheRS induced over-proliferation of ISCs. These phenotypes are not only independent of the aaRS activity (Fig 1D-F), they also do not reflect a function in sensing the availability of its enzymatic substrate Phe and transmitting this information to the major growth controller, the TOR pathway (Fig S3). The proliferation activity of α-PheRS is therefore fundamentally different from the growth supporting activity of the aaRS members TrpRS or LeuRS (Adam et al., 2018; Bonfils et al., 2012; Han et al., 2012).

Overexpression of α-PheRS in the gut ISCs additionally interfered with cell fate decisions by driving ISCs to duplicate and to differentiate into EEs. The combination of these effects results in a "tumor-like" phenotype, that had been described as ISC/EE tumor phenotype that results from downregulation of *Notch* activity (Korzelius et al., 2014; Micchelli and Perrimon, 2006). Interestingly, mis-regulating proteins involved in EE fate specification, like downregulation of Tramtrack69 or upregulation of its adaptor protein Phyllopod, also results in this phenotype (Wang et al., 2015; Yin and Xi, 2018), suggesting that α-PheRS levels, through their activity on Notch signaling, induce the "tumor-like" phenotype in the gut tissue not only by increasing stem cell proliferation, but also by driving differentiating cells into an EE fate.

The gut phenotype caused by elevated levels of α-PheRS points to the importance of controlling and fine tuning these levels. We found that the JAK/STAT pathway has the capability of modulating cellular α-PheRS levels. Interestingly, JAK/STAT signaling, which stimulates progenitor cell differentiation during normal tissue homeostasis (Herrera and Bach, 2019), downregulates *α-PheRS* levels, which consequently allows higher Notch signaling to promote differentiation of the EB progenitor cells into ECs. Therefore, regulation of α-PheRS levels links the two signaling pathways and implicates α-PheRS not only in promoting cell proliferation, but also in regulating stem cell and tissue homeostasis by connecting the Notch

421 to the JAK/STAT signaling pathway. Stat92E is a transcription factor, but none of the
422 published reports on Stat92E targets lists the *α-PheRS* gene (Bina et al., 2010; Muller et al.,
423 2005; Wang et al., 2013). A direct repression of *α-PheRS* gene expression by Stat92E appears
424 therefore unlikely, even though it is also possible that this interaction escaped detection because
425 it happens in too few cells of the analyzed cell types.

426 An interplay between the JAK/STAT and the Notch signaling pathways to maintain
427 ISC homeostasis has been noted before in regenerating midguts. In this situation, damaged ECs
428 release Upd cytokines to activate JAK/STAT signaling in ISCs and to promote ISC division
429 (Jiang et al., 2009). This also stimulates Delta/Notch activity to promote EC differentiation
430 (Jiang et al., 2009). Knocking down *Stat92E* reduced Notch signaling, and Notch target genes
431 were downregulated when *Stat92E* activity was abolished in progenitor cells (Jiang et al.,
432 2009). JAK/STAT signaling therefore feeds into the downstream Notch signaling pathway
433 under these conditions, too. Our work revealed an unexpected missing link between the two
434 signaling pathways in normal tissue homeostasis and it would therefore be interesting to also
435 explore the function of *α-PheRS* in these pathways during tissue regeneration.

436

437 **Relevance of moonlighting function of α-PheRS for tumor formation**

438 Several aaRSs have come into the focus of cancer research (Kim et al., 2014). For instance,
439 LeuRS senses the availability of the amino acid Leu and if these levels are sufficient to support
440 growth, it signals a growth readiness to the key growth controller TORC1/mTORC1 (Bonfils
441 et al., 2012; Han et al., 2012). Our results suggest that PheRS does not serve an analogous
442 function as a Phe sensor (Suppl. Figure S3). Phe binding appears to be dispensable to activate
443 proliferation and to repress *Notch* signaling because the α-PheRS^{Cys} mutant, in which two
444 essential residues in the Phe binding pocket were replaced by Cys is unable to perform

aminoacylation (presumably because it cannot bind Phe), but still able to induce the non-canonical activity.

Improper expression of PheRS was suspected long ago to promote carcinogenesis, but till now the mechanisms behind this effect remind unknown. Elevated levels of *FARSA/CML33* (human α-PheRS) during the development of myeloid leukemia have been demonstrated to directly correlate with tumorigenic events (Sen et al., 1997). The GENT2 database published in 2019 describes also strong positive correlations between PheRS subunit levels and tumorigenic events in several tissues and cancers, including colon cancer, which mostly seems to originate from intestinal stem cells (ISCs) (Barker et al., 2009). Modelling the effect of elevated α-PheRS levels in *Drosophila* ISCs and CBs, we found that these levels lead to over-proliferation of cells with stem cell characteristics and to changes in cell fate, indicating that elevated α-PheRS levels can indeed be a risk factor for tumor formation.

Modeling the effects of elevated α-PheRS levels in ISCs revealed that hyperaccumulation of stem cells, a tumor risk, is mediated by high α-PheRS repressing Notch signaling. In mammals, Notch signaling is essential for maintaining the homeostasis of cell proliferation and differentiation (Qiao and Wong, 2009), similar to the function of Notch signaling in the Drosophila gut that is needed to prevent the induction of enteroendocrine tumors characterized by excessive EEs and ISCs in the adult midgut (Micchelli and Perrimon, 2006; Ohlstein and Spradling, 2007). Because in human, mis-regulation of Notch signaling in these processes has been suggested to trigger the development of colon cancer, *Notch* has been proposed as a molecular target for cancer therapy (Yin et al., 2010). The results presented here provide new and unexpected insights into the communication between two major signaling pathways involved in gut tumorigenesis and they suggest new opportunities to target these mechanisms.

Materials and Methods

Key Resources Table

Reagent or Resource	Sources	Identifier	Additional information
Antibodies			
Anti phospho-Histone H3-rabbit	Cell signaling	9701S	1:200 v/v
Anti phospho-Histone H3-mouse	Cell signaling	9706S	1:200 v/v
Anti *α-PheRS*	Genescript	4668	Customized product (1:200 v/v)
Anti *α-PheRS*	Genescript	4669	Customized product (1:200 v/v)
Anti Myc-mouse	Developmental Studies Hybridoma Bank (DSHB)	9E10	Supernatant (1:3 v/v)
Anti Puromycin	DSHB	PMY-2A4	1:100 v/v
Anti Prospero	DSHB	MR1A	1:200 v/v
Anti Delta	DSHB	C594.9B	1:10 v/v
Anti V5 tag-rabbit	Cell signaling	13202	1:200 v/v
Anti Cy3 rabbit	Jackson Immuno Research	115-165-146	1:200 v/v
Anti-rabbit Alexa Flour 488	Molecular Probes	A-11008	1:200 v/v
Anti-rabbit Alexa Flour 488	Molecular Probes	A-11034	1:200 v/v
Anti-mouse Alexa Flour 488	Molecular Probes	A-11029	1:200 v/v
Anti-rabbit Alexa Flour 488	Life technology	A-21206	1:200 v/v
Anti-rabbit Alexa Flour 594	Invitrogen	A-11037	1:200 v/v
Anti-mouse Alexa Flour 594	Molecular Probes	A-11032	1:200 v/v
Anti-mouse Alexa Flour 568	Life technology	A-10037	1:200 v/v
Anti α-tubulin	Abcam	Ab18251	1:1,000 v/v
Anti GFP	ImmunoKontact	042704	1:1,000 v/v
Anti Myc-rabbit	Santa Cruz	Sc-789	A-12 (1:1,000 v/v)
HRP Anti rabbit IgG antibody (Peroxidase)	Vector	PI-1000	1:10,000 v/v
HRP Anti rabbit IgG antibody (Peroxidase)	Vector	PI-2000	1:10,000 v/v

Fly stocks and genetics			
α-PheRS^{G2060}/FM6	Bloomington Drosophila Stock Center (BDSC)	26625	
RNAi- α-PheRS	Vienna Drosophila RNAi Center (VDRC)	33514	
RNAi- β-PheRS	VDRC	42046	
eyeless-Gal4	BDSC	5535	
engrailed-Gal4	BDSC	30564	
UAS-GFP	BDSC	6658	
STAT92E[HJ]/TM3,Sb	BDSC	24510	
w; UAS-Myc::MYC	BDSC	9674	
hspFLP/y ; + ; UAS-Myc::MYC	BDSC	9675	
hspFLP/y ; UAS-N^{ICD}/CyO ; MKRS/TM2	BDSC	52008	
10X STAT92E GFP	BDSC	26197	
UAS-N RNAi	BDSC	33611	
UAS-N RNAi	BDSC	7078	
*neoFRT*82B *Sb1*/TM6	BDSC	2051	
NRE-EGFP	BDSC	30728	
UAS-Dl	BDSC	5614	
tub-Gal4/TM3,Sb	BDSC	5138	
y w att2A[vas-ϕ]; +; attP-86F	ETH Zurich		A gift from Hugo Stocker, ETH
esg-Gal4,UAS-2XEYFP;MKRS/TM6B,Tb	ETH Zurich		A gift from Hugo Stocker, ETH
yw; esg-Gal4, UAS-GFP/TM6B,Tb,Hu	ETH Zurich	2400	A gift from Hugo Stocker, ETH
NP1-Gal4 (Myo31DF)/CyO y+	ETH Zurich	2398	A gift from Hugo Stocker, ETH
esg-Gal4, UAS-mCherry-CD8, tub-gal80^{ts}/CyO			A gift from Péter Nagy, Cornell University
yw;UAS-cyto-gars-myc/CyO			A gift from Albena Jordanova, VIB-U Antwerp Center for Molecular Neurology

472

Bacteria strains and vectors		
XL1 blue	Aligent	200249
Rosseta – Novagen	Merckmilipore	70954
pET-28a – Novagen	Merckmilipore	69864
pET LIC (2A-T)	Addgene	29665
pUASattB	Drosophila Genomics Resource Center	1419
pw+SNattB	(Koch et al., 2009)	
Commercial assay or kit		
Pierce® Silver Stain kit	Thermo Scientific	24612
Pierce® BCA Protein Assay kit	Thermo Scientific	23227
ReliaPrep™ DNA CleanUp and Concentration System	Promega	A2893
GeneElute™ HP Plasmid miniprep kit	Sigma	NA0160
Qiagen® Plasmid Plus Midi kit	Qiagen	12943
Ni-NTA affinity resin	Qiagen	30210
ECL™ Prime Western Blotting System	GE Healthcare	RPN2232
RNAMaxx™ High Yield Transcription Kit	Aligent	200339
Software, algorithm		
Leica Application Suite X (LAS X)	Leica	https://www.leica-microsystems.com/products/microscope-software/p/leica-las-x-ls/
FIJI	ImageJ	https://fiji.sc/
GraphPad Prism	GraphPad	https://www.graphpad.com/scientific-software/prism/
FlowJo™	BD Biosciences	https://www.flowjo.com/
Microsoft Excel	Microsoft	https://products.office.com/en-us/excel

Buffers

Lysis buffer for Drosophila tissue	**Lysis buffer for bacteria**
20 mM Tris HCl pH7.4 150uM NaCl 2 mM EDTA 50 mM NaF 10% Glycerol 1% Triton X100 1 Protease inhibitor cocktail tablet (Roche-4693159001)	20 mM Tris HCl pH7.4 150uM NaCl 2 mM EDTA 50 mM NaF 10% Glycerol 1% Triton X100 4mM Imidazole 1M 0.6% Lysozyme

1 mM phenylmethylsulphonyl fluoride	1 Protease inhibitor cocktail tablet 1 mM phenylmethylsulphonyl fluoride
4% PFA	**1X PBST**
1X PBST 4% (w/v) Paraformaldehyde	0.2 % (v/v) Tween 20 1X PBS
Blocking buffer	**Fly food recipe**
5% (w/v) non-fat dry milk 0.1% (v/v) Triton X100	20.4 l H_20 1,680 g Maize flour 720 g Yeast 1,800 g Syrup 192 g Potassium sodium tartrate tetrahydrate 36 g Nipagin 120 ml Propionic acid
10X PBS pH 7.4	
10.6 mM KH_2PO_4 1.5 M NaCl 30 mM $Na_2PO_4.7H_20$	
10X SDS running buffer	**10X Transfer buffer**
30 g Tris base 144 g Glycine 10 g SDS dH_2O to 1ℓ	30 g Tris base 144 g Glycine dH_2O to 1ℓ
10X TBS pH to 7.6	**1X TBST**
24 g of Tris Base 88 g of NaCl dH_2O to 1ℓ	100 mL 10X TBS 900 mL dH_2O 0.1% (v/v) Tween 20

475

476 **Primers**

Name	**Sequence (5' to 3')**	**Application**
rc2263f	CGCGGATCCATCCGGCGAGAGAGTGTCTTTG	Genomic genomic construct of *α-PheRS*
rc2263r	CGGGGTACCTATGCCTGGCGATAATCGTG	
Tyr412Cys & Phe438Cys-F	TCAAGCCGGCGTACAATCCGTGTACCGAGCCCAG	Construct of *α-PheRS*^{Cys} mutation
Tyr412Cys & Phe438Cys-R	CTCCGGCCGACAGACGCCCGAGTTGCCC	
α-PheRS RNAi 11f	TAATACGACTCACTATAGGGAGGCAAGAAACGCAAGCTCCTC	*α-PheRS* ds RNA synthesis
α-PheRS RNAi 11r	TAATACGACTCACTATAGGGAGGGAACTCCGCCAGATGTGTG	
β-PheRS RNAi 10f	TAATACGACTCACTATAGGGAGGGCCAATCATTCGGGAATCA	*β-PheRS* ds RNA synthesis
β-PheRS RNAi 10r	TAATACGACTCACTATAGGGAGGAGGCAGGGACTTCTTAATGT	
seq r6	GCTCCCATTCATCAGTTCC	Sequencing
seqA r1	CATTTCCACCGTGAGATCCGTC	Sequencing
seqA r2	AACTCTTGTGGGTGACCGTTTC	Sequencing
seqA f1	GTTCTCGAAGTGAATGTTCTGG	Sequencing

seqA f2	TTTAGCCACCGTCGTCGTTTC	Sequencing
seqA r3	TCCAGCGACGATGACGAATTTG	Sequencing
seqA f3	CAAATGGATTGTGGGACCAGC	Sequencing
seqA r4	GCCCTCCTCCACCATCTTTAG	Sequencing

Fly genetics and husbandry

All *Drosophila melanogaster* fly stocks were kept for long term storage at 18ºC in glass or plastic vials on standard food with day/night (12h/12h) light cycles. All experiments were performed at 25ºC unless specifically mentioned. A UAS-GFP element was added in the crosses of all rescue experiments to even out the effect of Gal4 by providing the same number of UAS constructs. Origins of all stocks are noted in the *Key Resource Table*.

DNA cloning and generation of transgenic flies

Sequence information was obtained from Flybase. All mutations and the addition of the Myc-tag to the N-terminus of *α-PheRS* were made by following the procedure of the QuickChange® Site-Directed Mutagenesis Kit (Stratagene). The genomic *α-PheRS* rescue construct (*Myc::α-PheRS*) codes for the entire coding region and for an additional Myc tag at the N-terminal end. In addition, it contains ~ 1kb of up- and down-stream sequences and it was cloned into the *pw*$^{+}$*SNattB* transformation vector (Koch et al., 2009; Lu et al., 2014). The *α-PheRS* and *β-PheRS* cDNAs were obtained by RT-PCR from mRNA isolated from 4-8 days old *OreR* flies (Lu et al., 2014). The Tyr412Cys and Phe438Cys mutations in the *α-PheRS* sequence were created by site directed mutagenesis. Like the wild-type cDNA, they were cloned into the *pUASTattB* transformation vector to generate the pUAS-α-PheRS and pUAS-α-PheRS^{Cys}. Before injecting these constructs into fly embryos, all plasmids were verified by sequencing (Microsynth AG, Switzerland). Transgenic flies were generated by applying the ϕ C31-based integration system with the stock (*y w att2A[vas-ϕ]; +; attP-86F*) (Bischof et al., 2007).

499 **Western blotting**

500 Protein was extracted from tissues, whole larvae, or flies using the lysis buffer. Protein lysates
501 were separated by SDS-PAGE and transferred onto PVDF membranes (Milipore, US). The
502 blocking was performed for 1h at room temperature (RT) with non-fat dry milk (5%) in TBST
503 solution. Blots were probed first with primary antibodies (diluted in blocking buffer) overnight
504 at 4°C and then with secondary antibodies (diluted in TBST) 1h at RT. The signal of the
505 secondary antibody was detected by using the detect solution mixture (1:1) (ECL™ Prime
506 Western Blotting System, GE Healthcare Life Science) and a luminescent detector (Amersham
507 Imager 600, GE Healthcare Life Science). Origins and recipes of all buffers and reagents are
508 noted in *Key Resource Table*.

509

510 **Immunofluorescent staining and confocal microscopy**

511 Guts were dissected from each female fly 3 days after eclosure, and a total of 10 guts were
512 analyzed for each genotype. Dissections were performed in PBS 1X on ice and tissues were
513 collected within maximum one hour. Fixation with 4% PFA in PBS-T 0.2% at RT was done
514 for different durations depending on the different tissues: two hours (gut), 40 minutes (brain),
515 30 minutes (wing discs, ovary). Then the samples were blocked overnight with blocking buffer
516 at 4°C. Primary antibodies (diluted in blocking buffer) were incubated with the samples for 8h
517 at RT. The samples were rinsed 3 times and washed 3 times (20 minutes/wash) with PBST.
518 Secondary antibodies (diluted in PBST) were incubated overnight at 4°C. The samples were
519 then rinsed 3 times and washed 2 times (20 minutes/wash) with PBST. Hoechst 33258 (2.5
520 µg/ml) was added in PBST before the last washing step and the samples were mounted with
521 Aqua/Poly Mount solution (Polysciences Inc., US). For the anti-Delta labeling, the samples
522 were blocked for 3h at RT with blocking buffer. The primary anti-Delta antibody (1:10 v/v)

was incubated with the samples overnight at 4°C and then the secondary antibody was incubated overnight at 4°C. Origins and diluted concentrations of all buffers and antibodies are noted in *Key Resource Table*.

Protein synthesis measurements using the ribopuromycylation method (RPM)

For puromycin labeling experiments, tissues were dissected in Schneider's insect medium (Sigma, US) supplement with 10% fetal calf serum (FCS, Sigma, US) at 25°C. They were then incubated with Schneider's insect medium containing puromycin (5 µg/ml, Sigma, US) and cycloheximine (CHX, 100 µg/ml, Sigma, US) for 2 hours at RT. Then the samples were fixed with 4% PFA in PBS-T 0.2% at RT and blocked overnight with blocking buffer at 4°C. Primary anti-Puromycin antibody (diluted in PBST) was incubated with the samples for 8h at RT. The samples were rinsed 3 times and washed 3 times (20 minutes/wash) with PBST. Secondary antibodies (diluted in PBST) were incubated overnight at 4°C. The samples were then rinsed 3 times and washed 2 times (20 minutes/wash) with PBST. Hoechst 33258 (2.5 µg/ml) was added in PBST before the last washing step and the samples were mounted with Aqua/Poly Mount solution (Polysciences Inc., US).

***In vitro* aminoacylation assay**

Recombinant α-PheRS and β-PheRS proteins were expressed in the *E. coli* strain Rosetta (Novagen) and then purified (Moor et al., 2002). For this, the *α-PheRS* or *α-PheR*^{Cys} mutant cDNAs were cloned with His tags at the N-terminal end into the pET-28a plasmid expression vector (Novagen). Wild-type *β-PheRS* cDNAs were cloned into the pET LIC (2A-T) plasmid (Addgene). Then, His-α-PheRS or the His-α-PheR^{Cys} mutant and β-PheRS were co-expressed

546 in the *E. coli* strain Rosetta with isopropylthiogalactoside (IPTG, 1mM) induction at 25 °C for
547 6 hours. Proteins were purified with Ni-NTA affinity resin (Qiagen). The aminoacylation assay
548 protocol from Jiongming Lu was then followed (Lu et al., 2014). This assay was performed at
549 25 °C in a 100µl reaction mixture containing 50 mM Tris-HCl pH 7.5, 10 mM $MgCl_2$, 4 mM
550 ATP, 5 mM β-mercaptoethanol, 100 µg/ml BSA, 3 U/ml *E. coli* carrier tRNA, 5 µM [^{3}H]-
551 amino acid (L-Phe) and 1 µM $tRNA^{Phe}$ from brewer's yeast (Sigma, US). In each experiment,
552 a 15-µl aliquot was removed at four different incubation time points, spotted on a Whatman
553 filter paper discs and washed three times with ice-cold 5% trichloroacetic acid and once with
554 ice-cold ethanol. A blank paper disc without spotting and another with spotting the enzyme-
555 free reaction were used for detecting background signals. After filter discs were dried, they
556 were immersed into PPO Toluol (Sigma, US) solution in plastic bottles and the radioactivity
557 was measured by scintillation counting.

558

559 **Wing disc dissociation and FACS analysis**

560 Wandering larvae derived from 2-4 hours egg collections were dissected in PBS during a
561 maximal time of 30 minutes. Around twenty wing discs were incubated with gentle agitation
562 at 29°C for around 2-hours in 500µl 10× Trypsin-EDTA supplemented with 50 µl 10×Hank's
563 Balanced Salt Solution (HBSS) (Sigma, US) and 10 µl Vybrant DyeCycle Ruby stain
564 (Molecular Probes, US). Dissociated cells from wing discs were directly analyzed by FACS-
565 Calibur flow cytometer (Becton Dickinson, US).

566 *Drosophila* tissue culture cells were harvested and fixed in 70% ethanol and stained
567 with a staining solution containing 1mg/ml propidium iodide, 0.1% Triton and 10 mg/ml RNase
568 A. The cells were then subjected to FACS-Calibur cytometry and data were analyzed with the
569 FlowJo software.

570 ***Drosophila* cell culture and RNAi treatment**

571 The protocols for in vitro cell culture and RNAi treatment was described in the PhD thesis of
572 Jiongming Lu (Lu, 2013). *Drosophila* Kc cells were incubated at 25°C in Schneider's
573 *Drosophila* medium supplemented with 10% heat-inactivated fetal calf serum (FCS) and 50
574 µg/ml Penicillin/Streptomycin. To induce RNAi knockdown in *Drosophila* cells, dsRNA
575 treatment was performed (Clemens et al., 2000). dsRNAs around 500bp in length were
576 generated with the RNAMaxx^{TM} High Yield Transcription Kit (Agilent, US). Cells were
577 diluted to a concentration of 10^6 cells/ml in serum-free medium, and dsRNA was added directly
578 to the medium at a concentration of 15 µg/ml. The cells were incubated for 1 hour followed by
579 addition of medium containing FCS. Then the cells were kept in the incubator and were
580 harvested at different time points (1-5 days) after dsRNA treatment.

581

582 **Clonal assay and twin spot data analysis**

583 For twin spot tests, we used the Mosaic Analysis with a Repressible Cell Marker (MARCM)
584 system. Twin spots were generated with the progenitor genotype *hs-flp; tub-Gal4/UAS-β-*
585 *PheRS ; FRT82B, ubiGFP, UAS-α-PheRS$^{(Cys)}$/FRT82B Tub-Gal80.* In twin spots, the internal
586 control clone was GFP-minus and the sister clone with the red signal generated by the antibody
587 against the overexpressed protein. We induced the *hs-FLP*, *FRT82B* system at 37ºC for 1h on
588 the third day post-eclosure and dissected the animals 3 days post-induction. Confocal imaging
589 detected non-green clones (without ubiGFP) and red clones (stained with Myc antibody-red)
590 (Fig 9A).

591 In twin spots, cell numbers per clone were counted and the numbers of cell division per
592 clone were calculated as $\log_2$(cell numbers per clone). This represents the logarithm of the cell

593 numbers per clone to the base 2. The increase of cell proliferation (%) was analyzed by
594 comparing the number of cell divisions of the two clones in the same twin spot.

595

596 **Image acquisition and processing**

597 Imaging was carried out with a Leica SP8 confocal laser scanning microscope equipped with
598 a 405 nm diode laser, a 458, 476, 488, 496 and 514 nm Argon laser, a 561 nm diode pumped
599 solid state laser and a 633 nm HeNe laser. Images were obtained with 20x dry and 63x oil-
600 immersion objectives and 1024x1024 pixel format. Images were acquired using LAS X
601 software. The images of the entire gut were obtained by imaging at the standard size and then
602 merging maximal projections of Z-stacks with the Tiles Scan tool. Fluorescent intensity was
603 determined from FIJI software.

604

605 **Quantification of cell numbers per posterior midgut**

606 Z stack images through the width of the posterior midgut were acquired along the length of the
607 posterior midgut from the R4a compartment to midgut-hindgut junction. Maximum projections
608 of each Z stack were obtained, and the total number of each cell type was counted manually
609 and exported to Microsoft Excel and GraphPad Prism for further statistical analysis.

610

611 **Quantification and statistical analysis**

612 For quantifications of all experiments, *n* represents the number of independent biological
613 samples analyzed (the number of guts, the number of wing disc, the number of twin spots),
614 error bars represent standard deviation (SD). Statistical significance was determined using the
615 t-test or ANOVA as noted in the figure legends. They were expressed as P values. (*) denotes

616 $p < 0.05$, (**) denotes $p < 0.01$, (***) denotes $p < 0.001$, (****) denotes $p < 0.0001$. (*ns*)
617 denotes values whose difference was not significant.
618
619
620

621 ## Acknowledgements

622 We thank Peter Nagy, Hugo Stocker, Albena Jordanova, Erik Storkebaum and the
623 Bloomington Stock Center for fly stocks. We are also grateful to Mark Safro for suggesting
624 mutations that disrupt the phenylalanine binding site of α-PheRS. This work was supported
625 by the Novartis Foundation for Medical-Biological Research (#18A050), the Swiss National
626 Fund (project grant 31003A_173188) and the University/Canton of Bern.
627
628

629 ## Author contributions

630 T.H., J.L. and B.S. conceived the ideas and designed the experiments. T.H. conducted most
631 experiments and performed the analysis of the results. J.L. performed the loss-of-function
632 experiments of PheRS and the mTOR signaling tests, the adult wing measurements and the
633 FACS analysis, including analyzing their data. T.H., J.L. and B.S. wrote the manuscript.
634
635

636 ## Conflict of interests

637 The authors declare that they have no conflict of interest.

References

Ables, J.L., Breunig, J.J., Eisch, A.J., Rakic, P., 2011. Not(ch) just development: Notch signalling in the adult brain. Nature reviews. Neuroscience 12, 269-283.

Adam, I., Dewi, D.L., Mooiweer, J., Sadik, A., Mohapatra, S.R., Berdel, B., Keil, M., Sonner, J.K., Thedieck, K., Rose, A.J., Platten, M., Heiland, I., Trump, S., Opitz, C.A., 2018. Upregulation of tryptophanyl-tRNA synthethase adapts human cancer cells to nutritional stress caused by tryptophan degradation. Oncoimmunology 7, e1486353.

Antonellis, A., Oprescu, S.N., Griffin, L.B., Heider, A., Amalfitano, A., Innis, J.W., 2018. Compound heterozygosity for loss-of-function FARSB variants in a patient with classic features of recessive aminoacyl-tRNA synthetase-related disease. Human mutation 39, 834-840.

Bach, E.A., Ekas, L.A., Ayala-Camargo, A., Flaherty, M.S., Lee, H., Perrimon, N., Baeg, G.H., 2007. GFP reporters detect the activation of the Drosophila JAK/STAT pathway in vivo. Gene expression patterns : GEP 7, 323-331.

Barker, N., Ridgway, R.A., van Es, J.H., van de Wetering, M., Begthel, H., van den Born, M., Danenberg, E., Clarke, A.R., Sansom, O.J., Clevers, H., 2009. Crypt stem cells as the cells-of-origin of intestinal cancer. Nature 457, 608-611.

Bina, S., Wright, V.M., Fisher, K.H., Milo, M., Zeidler, M.P., 2010. Transcriptional targets of Drosophila JAK/STAT pathway signalling as effectors of haematopoietic tumour formation. EMBO reports 11, 201-207.

Bischof, J., Maeda, R.K., Hediger, M., Karch, F., Basler, K., 2007. An optimized transgenesis system for Drosophila using germ-line-specific phiC31 integrases. Proceedings of the National Academy of Sciences of the United States of America 104, 3312-3317.

Bonfils, G., Jaquenoud, M., Bontron, S., Ostrowicz, C., Ungermann, C., De Virgilio, C., 2012. Leucyl-tRNA synthetase controls TORC1 via the EGO complex. Molecular cell 46, 105-110.

Buchon, N., Broderick, N.A., Chakrabarti, S., Lemaitre, B., 2009. Invasive and indigenous microbiota impact intestinal stem cell activity through multiple pathways in Drosophila. Genes & development 23, 2333-2344.

Casas-Tinto, S., Lolo, F.N., Moreno, E., 2015. Active JNK-dependent secretion of Drosophila Tyrosyl-tRNA synthetase by loser cells recruits haemocytes during cell competition. Nature communications 6, 10022.

Chen, J., Larochelle, S., Li, X., Suter, B., 2003. Xpd/Ercc2 regulates CAK activity and mitotic progression. Nature 424, 228-232.

672 Clemens, J.C., Worby, C.A., Simonson-Leff, N., Muda, M., Maehama, T., Hemmings, B.A.,
673 Dixon, J.E., 2000. Use of double-stranded RNA interference in Drosophila cell lines to
674 dissect signal transduction pathways. Proceedings of the National Academy of Sciences 97,
675 6499-6503.

676 de la Pompa, J.L., Wakeham, A., Correia, K.M., Samper, E., Brown, S., Aguilera, R.J.,
677 Nakano, T., Honjo, T., Mak, T.W., Rossant, J., Conlon, R.A., 1997. Conservation of the
678 Notch signalling pathway in mammalian neurogenesis. Development 124, 1139-1148.

679 Deliu, L.P., Ghosh, A., Grewal, S.S., 2017. Investigation of protein synthesis in Drosophila
680 larvae using puromycin labelling. Biology open 6, 1229-1234.

681 Dolde, C., Lu, J., Suter, B., 2014. Cross Talk between Cellular Regulatory Networks
682 Mediated by Shared Proteins. Advances in Biology 2014, 12.

683 Finarov, I., Moor, N., Kessler, N., Klipcan, L., Safro, M.G., 2010. Structure of human
684 cytosolic phenylalanyl-tRNA synthetase: evidence for kingdom-specific design of the active
685 sites and tRNA binding patterns. Structure 18, 343-353.

686 Giachino, C., Taylor, V., 2014. Notching up neural stem cell homogeneity in homeostasis and
687 disease. Frontiers in neuroscience 8, 32.

688 Gomard-Mennesson, E., Fabien, N., Cordier, J.F., Ninet, J., Tebib, J., Rousset, H., 2007.
689 Clinical significance of anti-histidyl-tRNA synthetase (Jo1) autoantibodies. Annals of the
690 New York Academy of Sciences 1109, 414-420.

691 Grandbarbe, L., Bouissac, J., Rand, M., Hrabe de Angelis, M., Artavanis-Tsakonas, S.,
692 Mohier, E., 2003. Delta-Notch signaling controls the generation of neurons/glia from neural
693 stem cells in a stepwise process. Development 130, 1391-1402.

694 Greenberg, Y., King, M., Kiosses, W.B., Ewalt, K., Yang, X., Schimmel, P., Reader, J.S.,
695 Tzima, E., 2008. The novel fragment of tyrosyl tRNA synthetase, mini-TyrRS, is secreted to
696 induce an angiogenic response in endothelial cells. FASEB journal : official publication of
697 the Federation of American Societies for Experimental Biology 22, 1597-1605.

698 Guo, M., Schimmel, P., 2013. Essential nontranslational functions of tRNA synthetases.
699 Nature chemical biology 9, 145-153.

700 Han, J.M., Jeong, S.J., Park, M.C., Kim, G., Kwon, N.H., Kim, H.K., Ha, S.H., Ryu, S.H.,
701 Kim, S., 2012. Leucyl-tRNA synthetase is an intracellular leucine sensor for the mTORC1-
702 signaling pathway. Cell 149, 410-424.

703 Hariharan, I.K., 2015. Organ Size Control: Lessons from Drosophila. Developmental cell 34,
704 255-265.

705 Hatakeyama, J., Bessho, Y., Katoh, K., Ookawara, S., Fujioka, M., Guillemot, F., Kageyama,
706 R., 2004. Hes genes regulate size, shape and histogenesis of the nervous system by control of
707 the timing of neural stem cell differentiation. Development 131, 5539-5550.

708 Herrera, S.C., Bach, E.A., 2019. JAK/STAT signaling in stem cells and regeneration: from
709 Drosophila to vertebrates. Development 146.

710 Housden, B.E., Millen, K., Bray, S.J., 2012. Drosophila Reporter Vectors Compatible with
711 PhiC31 Integrase Transgenesis Techniques and Their Use to Generate New Notch Reporter
712 Fly Lines. G3 (Bethesda) 2, 79-82.

713 Jiang, H., Patel, P.H., Kohlmaier, A., Grenley, M.O., McEwen, D.G., Edgar, B.A., 2009.
714 Cytokine/Jak/Stat signaling mediates regeneration and homeostasis in the Drosophila midgut.
715 Cell 137, 1343-1355.

716 Kim, D., Kwon, N.H., Kim, S., 2014. Association of aminoacyl-tRNA synthetases with
717 cancer. Topics in current chemistry 344, 207-245.

718 Ko, Y.G., Kang, Y.S., Kim, E.K., Park, S.G., Kim, S., 2000. Nucleolar localization of human
719 methionyl-tRNA synthetase and its role in ribosomal RNA synthesis. The Journal of cell
720 biology 149, 567-574.

721 Ko, Y.G., Kim, E.Y., Kim, T., Park, H., Park, H.S., Choi, E.J., Kim, S., 2001. Glutamine-
722 dependent antiapoptotic interaction of human glutaminyl-tRNA synthetase with apoptosis
723 signal-regulating kinase 1. The Journal of biological chemistry 276, 6030-6036.

724 Koch, R., Ledermann, R., Urwyler, O., Heller, M., Suter, B., 2009. Systematic functional
725 analysis of Bicaudal-D serine phosphorylation and intragenic suppression of a female sterile
726 allele of BicD. PloS one 4, e4552.

727 Korzelius, J., Naumann, S.K., Loza-Coll, M.A., Chan, J.S., Dutta, D., Oberheim, J., Glasser,
728 C., Southall, T.D., Brand, A.H., Jones, D.L., Edgar, B.A., 2014. Escargot maintains stemness
729 and suppresses differentiation in Drosophila intestinal stem cells. The EMBO journal 33,
730 2967-2982.

731 Laplante, M., Sabatini, D.M., 2012. mTOR signaling in growth control and disease. Cell 149,
732 274-293.

733 Lee, S.W., Cho, B.H., Park, S.G., Kim, S., 2004. Aminoacyl-tRNA synthetase complexes:
734 beyond translation. Journal of cell science 117, 3725-3734.

735 Lin, G., Xu, N., Xi, R., 2010. Paracrine unpaired signaling through the JAK/STAT pathway
736 controls self-renewal and lineage differentiation of drosophila intestinal stem cells. Journal of
737 molecular cell biology 2, 37-49.

738 Ling, J., Yadavalli, S.S., Ibba, M., 2007. Phenylalanyl-tRNA synthetase editing defects result
739 in efficient mistranslation of phenylalanine codons as tyrosine. RNA 13, 1881-1886.

740 Lu, J., 2013. Phenylalanyl tRNA synthetase: functions in and beyond aminoacylation,
741 Institute of Cell Biology. University of Bern, Bern, Switzerland.

742 Lu, J., Bergert, M., Walther, A., Suter, B., 2014. Double-sieving-defective aminoacyl-tRNA
743 synthetase causes protein mistranslation and affects cellular physiology and development.
744 Nature communications 5, 5650.

745 Markowitz, S.D., Bertagnolli, M.M., 2009. Molecular origins of cancer: Molecular basis of
746 colorectal cancer. The New England journal of medicine 361, 2449-2460.

747 Martin, F.A., Morata, G., 2006. Compartments and the control of growth in the Drosophila
748 wing imaginal disc. Development 133, 4421-4426.

749 Micchelli, C.A., Perrimon, N., 2006. Evidence that stem cells reside in the adult Drosophila
750 midgut epithelium. Nature 439, 475-479.

751 Moor, N., Linshiz, G., Safro, M., 2002. Cloning and expression of human phenylalanyl-tRNA
752 synthetase in Escherichia coli: comparative study of purified recombinant enzymes. Protein
753 expression and purification 24, 260-267.

754 Muller, P., Kuttenkeuler, D., Gesellchen, V., Zeidler, M.P., Boutros, M., 2005. Identification
755 of JAK/STAT signalling components by genome-wide RNA interference. Nature 436, 871-
756 875.

757 Nathanson, L., Deutscher, M.P., 2000. Active aminoacyl-tRNA synthetases are present in
758 nuclei as a high molecular weight multienzyme complex. The Journal of biological chemistry
759 275, 31559-31562.

760 Niehues, S., Bussmann, J., Steffes, G., Erdmann, I., Kohrer, C., Sun, L., Wagner, M.,
761 Schafer, K., Wang, G., Koerdt, S.N., Stum, M., Jaiswal, S., RajBhandary, U.L., Thomas, U.,
762 Aberle, H., Burgess, R.W., Yang, X.L., Dieterich, D., Storkebaum, E., 2015. Impaired protein
763 translation in Drosophila models for Charcot-Marie-Tooth neuropathy caused by mutant
764 tRNA synthetases. Nature communications 6, 7520.

765 Ohlstein, B., Spradling, A., 2007. Multipotent Drosophila intestinal stem cells specify
766 daughter cell fates by differential notch signaling. Science 315, 988-992.

767 Otani, A., Slike, B.M., Dorrell, M.I., Hood, J., Kinder, K., Ewalt, K.L., Cheresh, D.,
768 Schimmel, P., Friedlander, M., 2002. A fragment of human TrpRS as a potent antagonist of
769 ocular angiogenesis. Proceedings of the National Academy of Sciences of the United States
770 of America 99, 178-183.

771 Patel, P.H., Dutta, D., Edgar, B.A., 2015. Niche appropriation by Drosophila intestinal stem
772 cell tumours. Nature cell biology 17, 1182-1192.

773 Qiao, L., Wong, B.C., 2009. Role of Notch signaling in colorectal cancer. Carcinogenesis 30,
774 1979-1986.

775 Roy, H., Ibba, M., 2006. Phenylalanyl-tRNA synthetase contains a dispensable RNA-binding
776 domain that contributes to the editing of noncognate aminoacyl-tRNA. Biochemistry 45,
777 9156-9162.

778 Schimmel, P.R., Soll, D., 1979. Aminoacyl-tRNA synthetases: general features and
779 recognition of transfer RNAs. Annual review of biochemistry 48, 601-648.

780 Sen, S., Zhou, H., Ripmaster, T., Hittelman, W.N., Schimmel, P., White, R.A., 1997.
781 Expression of a gene encoding a tRNA synthetase-like protein is enhanced in tumorigenic
782 human myeloid leukemia cells and is cell cycle stage- and differentiation-dependent.
783 Proceedings of the National Academy of Sciences of the United States of America 94, 6164-
784 6169.

785 Smirnova, E.V., Lakunina, V.A., Tarassov, I., Krasheninnikov, I.A., Kamenski, P.A., 2012.
786 Noncanonical functions of aminoacyl-tRNA synthetases. Biochemistry. Biokhimiia 77, 15-
787 25.

788 Takashima, S., Adams, K.L., Ortiz, P.A., Ying, C.T., Moridzadeh, R., Younossi-Hartenstein,
789 A., Hartenstein, V., 2011. Development of the Drosophila entero-endocrine lineage and its
790 specification by the Notch signaling pathway. Developmental biology 353, 161-172.

791 Tzima, E., Reader, J.S., Irani-Tehrani, M., Ewalt, K.L., Schwartz, M.A., Schimmel, P., 2005.
792 VE-cadherin links tRNA synthetase cytokine to anti-angiogenic function. The Journal of
793 biological chemistry 280, 2405-2408.

794 Wang, C., Guo, X., Dou, K., Chen, H., Xi, R., 2015. Ttk69 acts as a master repressor of
795 enteroendocrine cell specification in Drosophila intestinal stem cell lineages. Development
796 142, 3321-3331.

797 Wang, H., Chen, X., He, T., Zhou, Y., Luo, H., 2013. Evidence for tissue-specific Jak/STAT
798 target genes in Drosophila optic lobe development. Genetics 195, 1291-1306.

799 Wu, J.S., Luo, L., 2006. A protocol for mosaic analysis with a repressible cell marker
800 (MARCM) in Drosophila. Nature protocols 1, 2583-2589.

801 Wullschleger, S., Loewith, R., Hall, M.N., 2006. TOR signaling in growth and metabolism.
802 Cell 124, 471-484.

803 Yannay-Cohen, N., Carmi-Levy, I., Kay, G., Yang, C.M., Han, J.M., Kemeny, D.M., Kim,
804 S., Nechushtan, H., Razin, E., 2009. LysRS serves as a key signaling molecule in the immune
805 response by regulating gene expression. Molecular cell 34, 603-611.

806 Yin, C., Xi, R., 2018. A Phyllopod-Mediated Feedback Loop Promotes Intestinal Stem Cell
807 Enteroendocrine Commitment in Drosophila. Stem cell reports 10, 43-57.

808 Yin, L., Velazquez, O.C., Liu, Z.J., 2010. Notch signaling: emerging molecular targets for
809 cancer therapy. Biochemical pharmacology 80, 690-701.

810 Zhou, J.J., Wang, F., Xu, Z., Lo, W.S., Lau, C.F., Chiang, K.P., Nangle, L.A., Ashlock,
811 M.A., Mendlein, J.D., Yang, X.L., Zhang, M., Schimmel, P., 2014. Secreted histidyl-tRNA
812 synthetase splice variants elaborate major epitopes for autoantibodies in inflammatory
813 myositis. The Journal of biological chemistry 289, 19269-19275.

814

815

Figure legends:

Figure 1: *α–PheRS* overexpression increases numbers of mitotic cells without stimulating translation.

(A-B’’’,C) Wing disc phenotypes induced by the overexpression of α-*PheRS* or α-*PheRS*^{Cys}. *en-Gal4* was used to drive transgene expression in the posterior compartment of developing wing discs. Mitotic cells were labelled with anti-phospho-Histone H3 (PH3) antibodies (A: anterior compartment; P: posterior compartment). n=10, *p<0.05, **p<0.01 in t-test. (D-E”,F) Protein synthesis did not increase upon overexpression of *α-PheRS* or *α-PheRS* and *β-PheRS* together. *en-Gal4* was used to drive the overexpression of the transgenes in the posterior compartment of wing discs. dMyc was used as positive control. Protein synthesis was measured by the mean intensity of the puromycin (PMY) signal labelling the nascent polypeptides. n=15, ****p<0.0001, *ns:* not significant.

Figure 2: PheRS overexpression in wing discs induces excessive cell growth.

(A,B) PheRS overexpression increases wing size. One wing was chosen from each female fly, and a total of 20 wings were analyzed for each genotype. Quantification of wing size was performed by counting the pixels in both anterior (A) and posterior (P) compartments of the wing and calculating their ratio (P/A). PheRS overexpression of both subunits, but not a single subunit alone, increases wing size. GlyRS overexpression did not increase wing size, but slightly decreased it. Note that only the upper section of the y axis is shown. n=20, **, p<0.01 in t-test.

Figure 3: The proliferative activity of the *α-PheRS* subunit is independent of PheRS complex formation and tRNA^{Phe} aminoacylation.

839 Clonal analysis (twin spot) experiment of the effect of overexpression of the PheRS subunits in follicle
840 cells by the MARCM technique. After inducing mitotic recombination by expressing the flippase
841 under the control of the heat-shock (*hs*) promoter at 37ºC for 40 minutes, a recombining cell will
842 divide and give rise to two proliferating clones. (A) One clone (red) overexpresses PheRS and its twin
843 clone (GFP^- signal) does not and expresses normal levels (internal control, outlined with yellow line).
844 (B) Three days after inducing the recombination, the average number of cell divisions were calculated
845 for each clone and compared to its twin spot to obtain the proliferation increase (%). n= 30, **p<0.01,
846 ***p<0.001, ****p<0.0001 in ANOVA test.

847

848 **Figure 4: α-PheRS promotes ISC proliferation in the midgut.**

849 (A) The number of ISC clusters increased upon overexpression of *Myc::α-PheRS* in ISCs and EBs
850 (Esg^+-cells) of the larval gut. n=10, *p<0.05,****p<0.0001. (B) The cell number per Esg^+ cluster
851 increased upon overexpression of *Myc::α-PheRS* with the same *esg-Gal4* driver used in (A). Esg^+
852 clusters were categorized according to the number of cells per cluster. The fraction of big clusters (cell
853 number > 5) increased upon overexpression of *Myc::α-PheRS*. In contrast, the overexpression of *β-*
854 *PheRS::V5* alone or the overexpression of *β-PheRS::V5* together with *Myc::α-PheRS* showed the
855 same frequency of the different clusters as the wild type. (C-G) Whole gut images and pictures of the
856 posterior midgut area (C'-G') showing the different cells observed. The expression of the different
857 genes indicated were driven with the same driver used in (A). The eYFP signal (YFP) displayed in
858 green marks ISCs and EBs, Hoechst (blue) stains the DNA in the nuclei. Overexpression of the *α-*
859 $PheRS^{Cys}$ mutant gave rise to tumor-like areas in both the anterior and the posterior midgut (outlined
860 with dashed lines). (H) Mitotic cells were labelled with anti-phospho-Histone H3 (PH3) antibodies.
861 n=10, ****p<0.0001 in t-test. (I) Total cells per intestinal region were measured by counting Hoechst
862 33258 labeled cells manually. n=10, ****p<0.0001. (J-J") The overexpression of *α-PheRS* or *α-*
863 $PheRS^{Cys}$ with the *esg-Gal4* driver in adult guts also resulted in an over-proliferation phenotype of
864 Esg^+ stem cells and progenitor cells.

Figure 5: Elevated α-PheRS levels increase EE differentiation in the gut through downregulating Notch signaling.

(A-B,C) Overexpression of *α-PheRS*^{Cys} using the *esg-Gal4,UAS-2XEYFP* system led to an increase in the number of EEs compared to the ECs in both larval and adult guts. EEs were marked by anti-Prospero antibody, Hoechst-labelled polyploid cells were counted as ECs. Guts were dissected from female flies 3 days after eclosure, and at least 10 guts were analyzed for each genotype. n=10, ****p<0.0001. (A",B") The co-overexpression of *α-PheRS*^{Cys} with *Notch* rescued the over-proliferation of Esg^{+} cells as well as the EE/EC ratio.

(D-E') Whole adult gut images (D,E) and the posterior midgut area (D',E'). The same *esg-Gal4* driver marks ISCs and EBs (eYFP signal shown in green), Hoechst (blue) stains nuclear DNA. The *Notch* knockdown phenotype in the posterior midgut (outlined with dashed lines) is indistinguishable from the *α-PheRS*^{Cys} overexpression phenotype. Co-overexpression of *α-PheRS*^{Cys} with *Notch* rescued the midgut phenotype. (F) Notch activity reporter (NRE-EGFP) levels drastically decrease upon *α-PheRS* or *α-PheRS*^{Cys} overexpression in adult midgut ISCs that expresses GFP under the control of a Notch response element (NRE). The guts were dissected from female flies 3 days after eclosure. Protein lysates were then extracted and separated by SDS-PAGE gel. 25 guts were analyzed for each genotype.

Figure 6: High levels of *α-PheRS* repress neuroblast proliferation by downregulating the *Notch* pathway.

(A-A") The overexpression of *α-PheRS* or *α-PheRS*^{Cys} in neuroblasts reduced the ratio central brain (CB) size to optic lobe (OL) size. The *insc-Gal4,UAS-GFP* system was used to overexpress proteins in neuroblasts (NBs). NBs were labelled by GFP expression. Central brain (right area with GFP^{+} NBs) area is outlined by a white dashed line. (B) Effect of overexpression and knock down of *α-*

890 *PheRS*$^{(Cys)}$and *Notch* on the CB/OL size ratio. n=20, ***p<0.001, *ns*: not significant. (C) The larval
891 brains were dissected from third instar larvae, and at least 20 brains were analyzed for each genotype.
892 Each brain lobe was classified according to the number of type II NBs per brain lobe. The
893 overexpression of *α-PheRS* or *α-PheRS*^{Cys} reduced the number of type II NBs per brain lobe, and less
894 than half of the lobes contained the normal 7-8 NBs. *Notch RNAi* caused the same phenotype with
895 higher expressivity. Overexpressing *Notch* together with *α-PheRS*^{Cys} rescued the loss of NB phenotype
896 to normal wild-type levels. n = 25.

897

898 **Figure 7: The JAK/STAT transcription factor Stat92E regulates α-PheRS levels.**

899 (A-C'') Hypomorphic *Stat92E*^{HJ} mutants contain high levels of α-PheRS in their ISCs (B). Anti-Delta
900 antibody was used to label ISCs, and anti-α-PheRS was used to stain for α-PheRS. *esg-Gal4,UAS-*
901 *2XEYFP* was used to drive YFP expression (A-A'', control) and *Stat92E* RNAi (C-C''), respectively,
902 in ISCs and EBs. The white arrows indicate polyploid ECs with high levels of α-PheRS. (D-F') The
903 quantification of the signal in the image (A",B",C") is based on the line across the nucleus of the cell.
904 The signal intensity of α-PheRS differs between the ISC/EB (high) and distant EC (low) while the
905 signal intensity of α-PheRS is similar between the ISC/EB (high) and the neighboring EC (high). (G)
906 Suppressing the JAK/STAT signaling with the hypomorphic *Stat92E*^{HJ} allele or by RNAi significantly
907 elevated the levels of α-PheRS in ISCs/EBs and neighboring ECs (Nb EC), but not in distant ECs. α-
908 PheRS levels were measured by the mean intensity of the fluorescent signal. n=10, ****p<0.0001, *ns:*
909 not significant. (H-I'') The overexpression of Stat92E decreased α-PheRS levels in Esg^{+} cells (circled
910 with white dashed lines) in adult guts. The same setting was used as in (A). (J-K''') The *Stat92E*
911 activity did not alter upon overexpression of α-PheRS. The *10X STAT92E-GFP* reporter was used to
912 measure *Stat92E* activity. It expresses GFP under the control of 10 Stat92E binding sites. The *esg-*
913 *Gal4,UAS-mCD8:mCherry,tub-Gal80*^{ts} *system* was used to overexpress *α-PheRS* in ISCs and EBs.
914 The female flies were collected 3 days after eclosure and cultured at 29ºC for 7 days before dissecting
915 and harvesting their midguts.

Figure 1

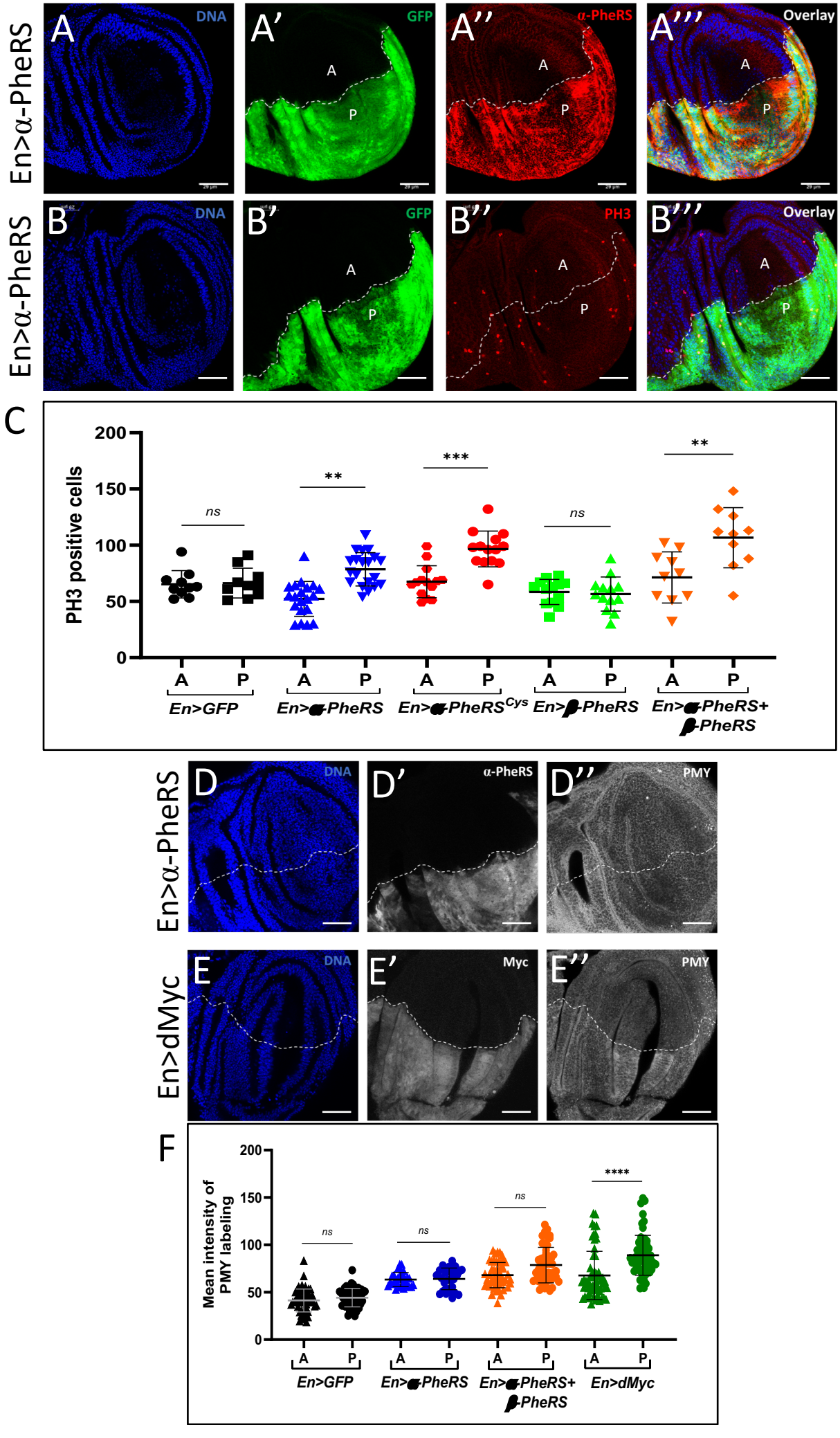

Figure 2

A

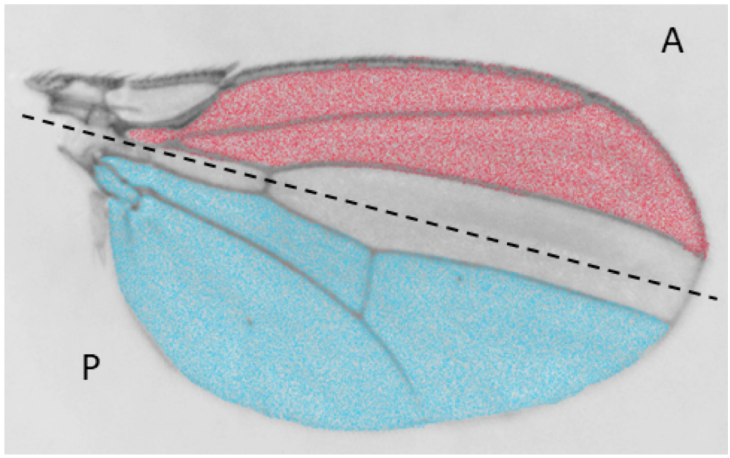

B

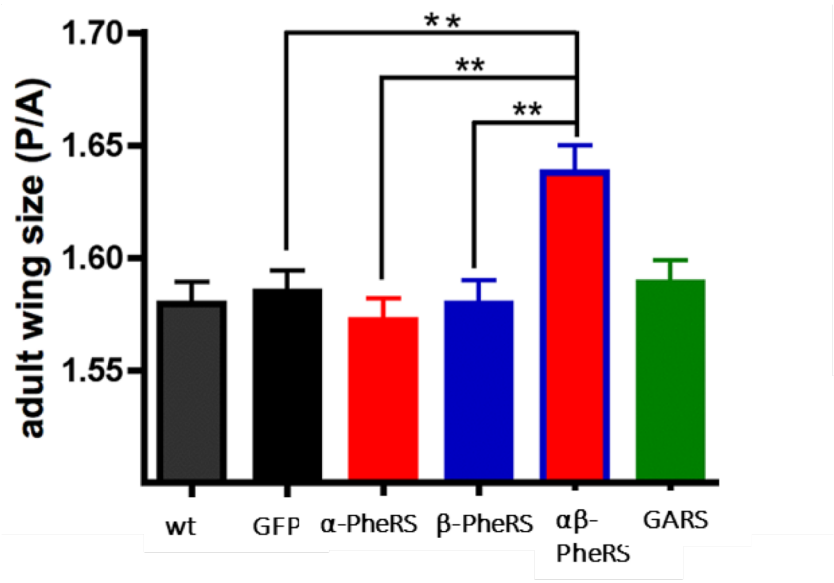

Figure 3

A

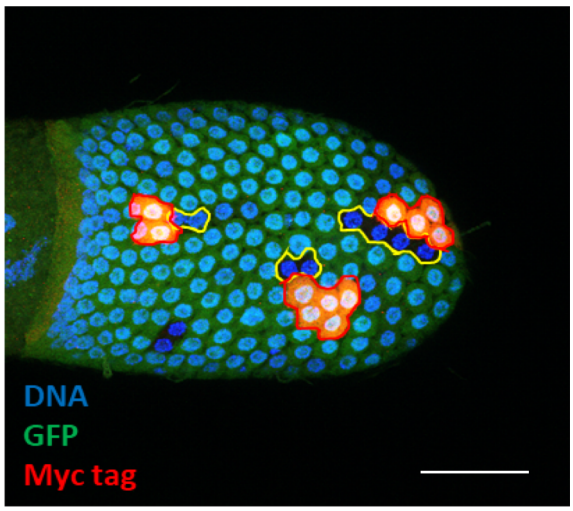

B

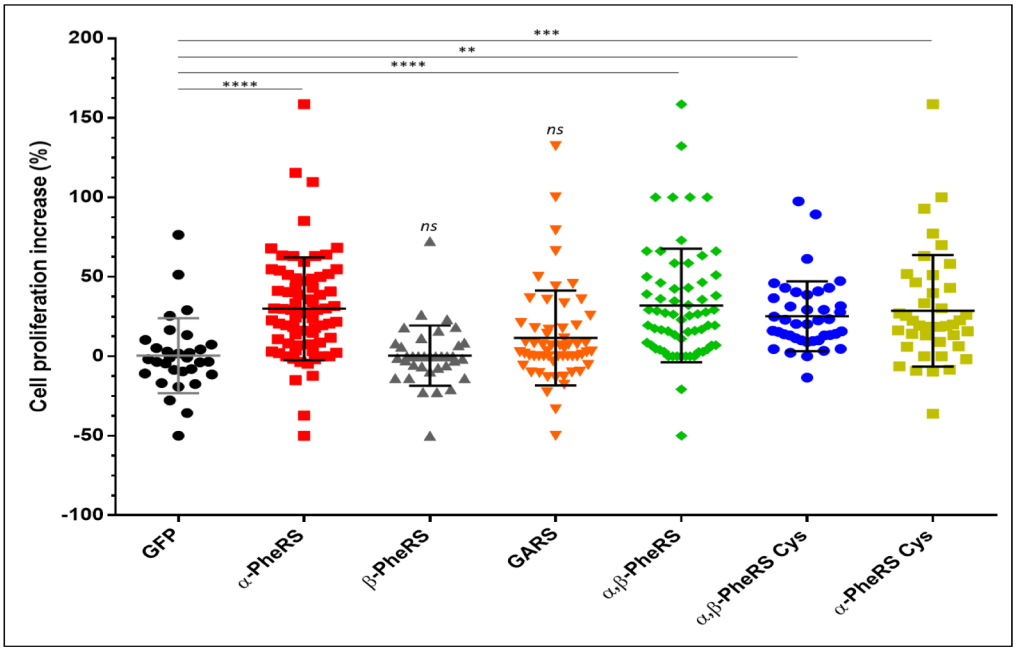

Figure 4

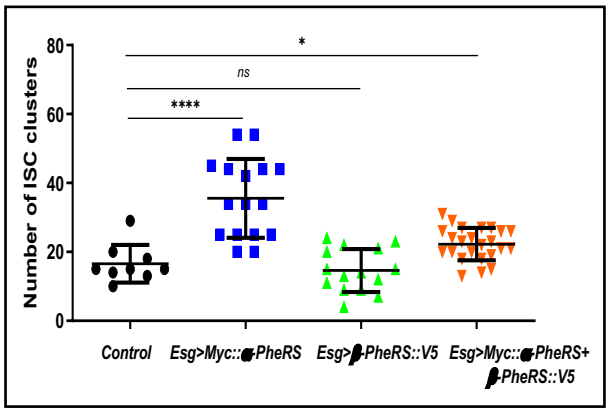

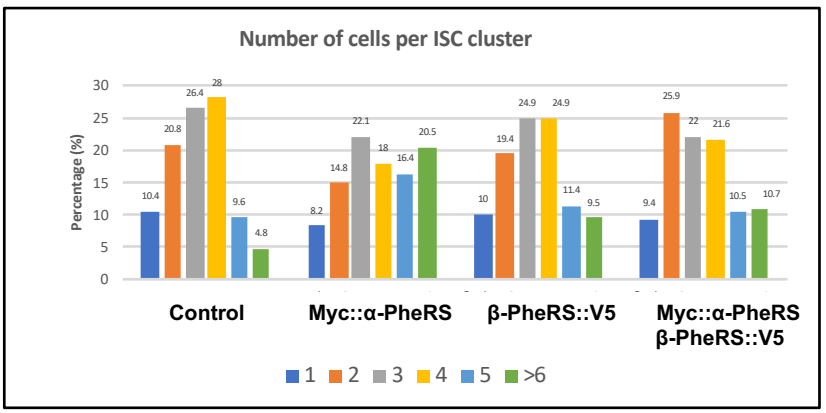

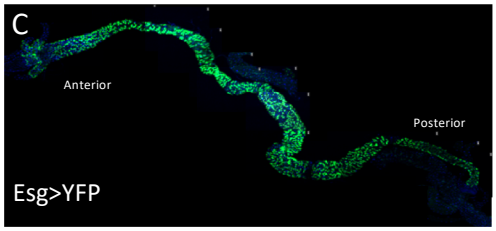

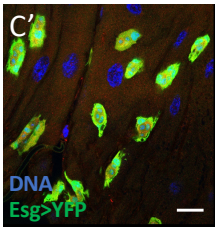

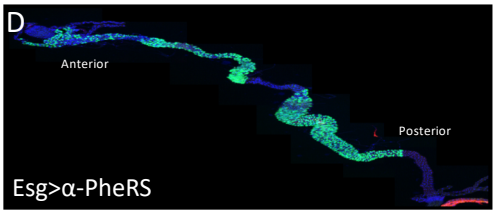

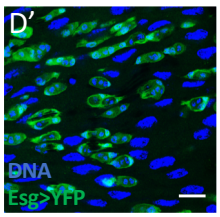

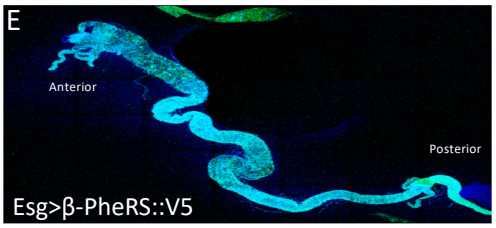

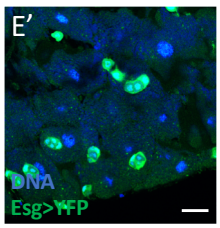

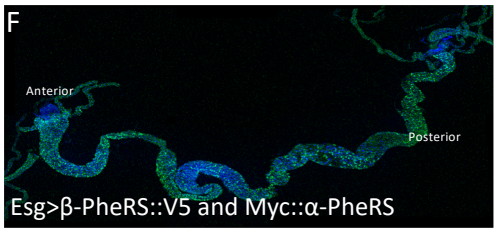

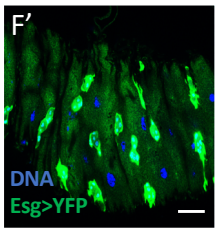

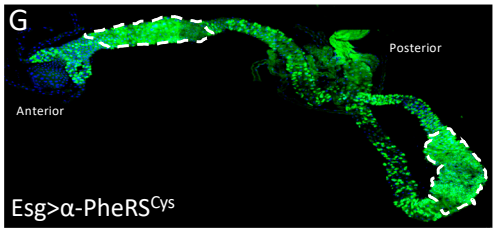

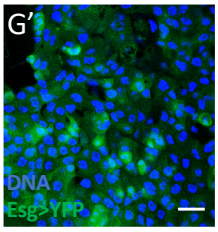

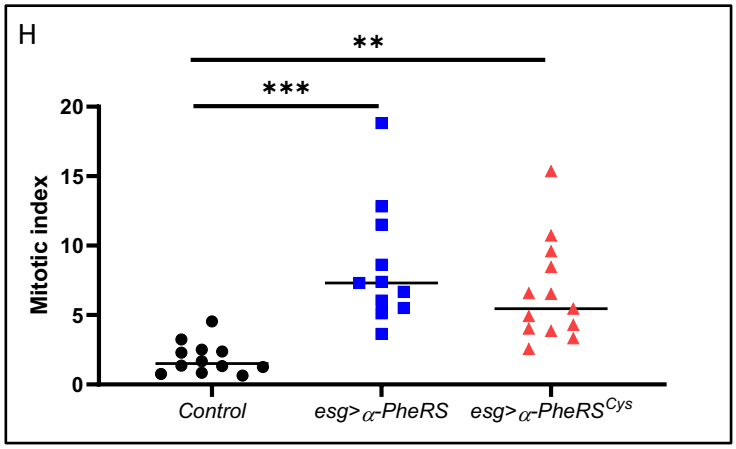

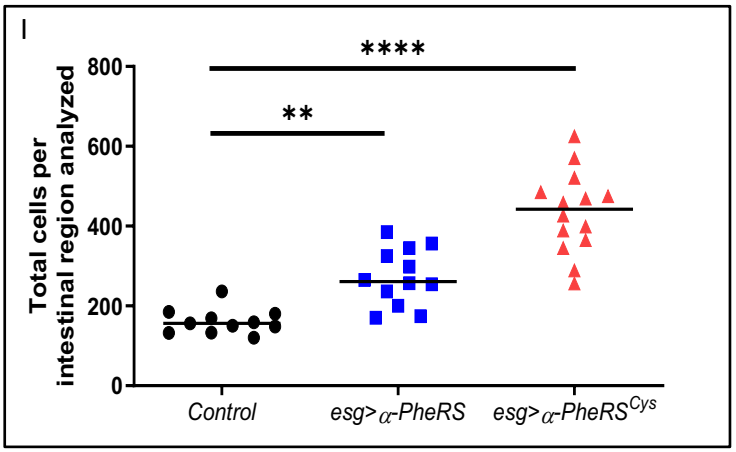

Adult midgut

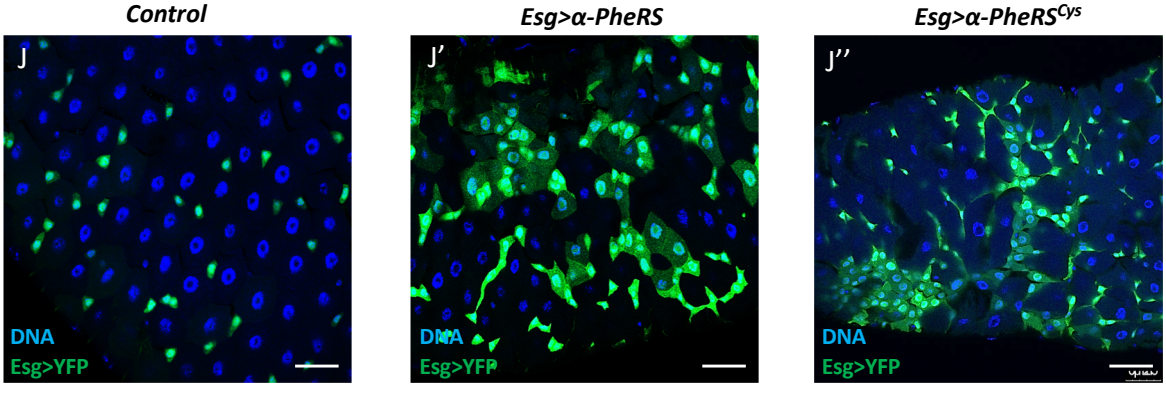

Figure 5

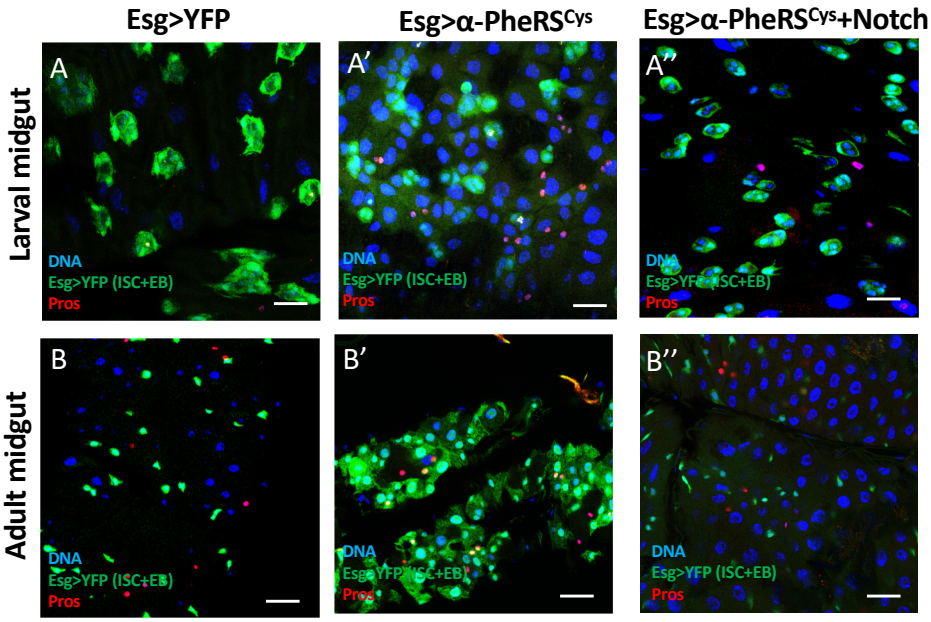
Esg>YFP
Esg>α-PheRS^Cys
Esg>α-PheRS^Cys+Notch
Larval midgut
Adult midgut
A
A'
A''
B
B'
B''
DNA
Esg>YFP (ISC+EB)
Pros

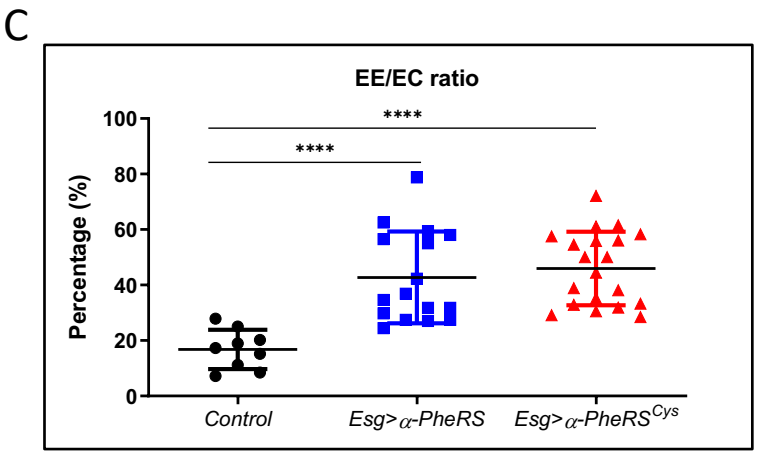
C
EE/EC ratio
****
****
Percentage (%)
100
80
60
40
20
0
Control
Esg>α-PheRS
Esg>α-PheRS^Cys

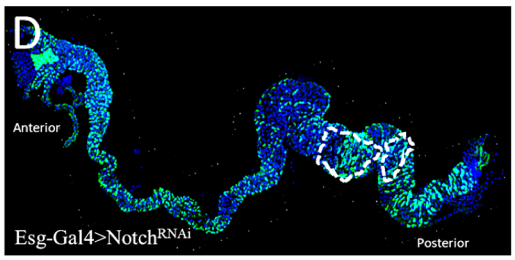
D
Anterior
Esg-Gal4>Notch^RNAi
Posterior

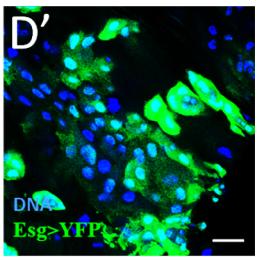
D'
DNA
Esg>YFP

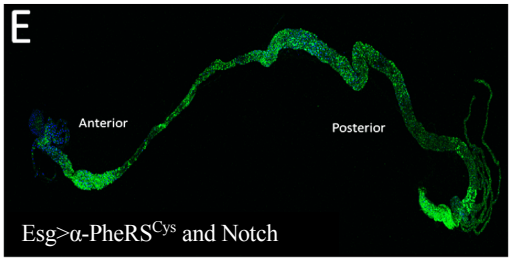
E
Anterior
Posterior
Esg>α-PheRS^Cys and Notch

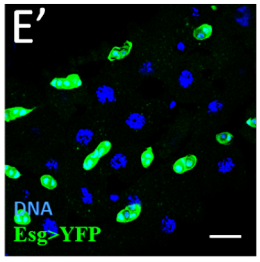
E'
DNA
Esg>YFP

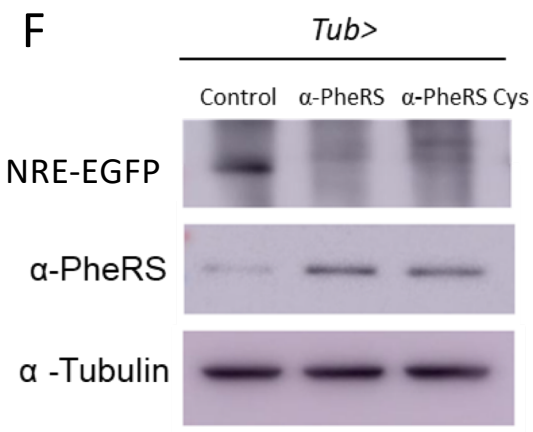
F
Tub>
Control
α-PheRS
α-PheRS Cys
NRE-EGFP
α-PheRS
α -Tubulin

Figure 6

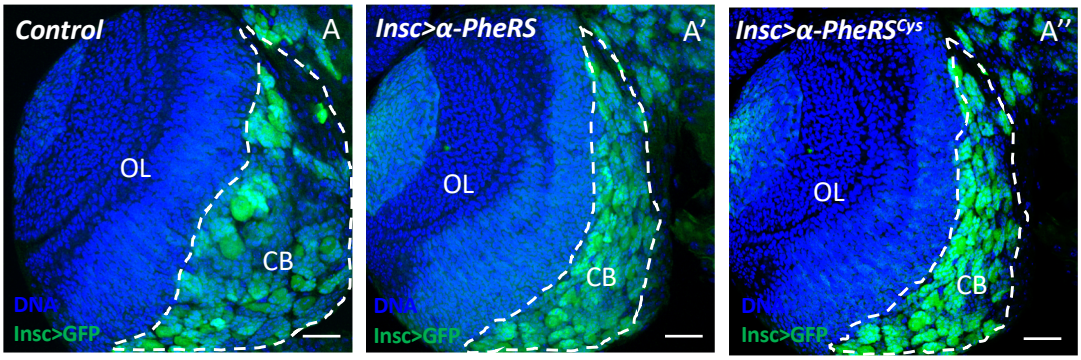
Control
A
OL
CB
DNA
Insc>GFP
Insc>α-PheRS
A'
OL
CB
DNA
Insc>GFP
Insc>α-PheRS^Cys
A''
OL
CB
DNA
Insc>GFP

B

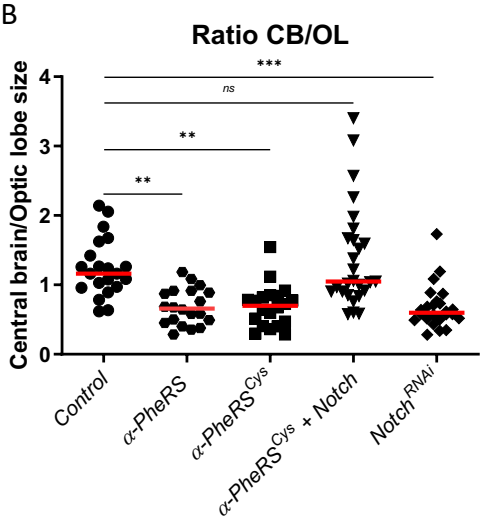
Ratio CB/OL
Central brain/Optic lobe size
0
1
2
3
4
***
ns
**
**
Control
α-PheRS
α-PheRS^Cys
α-PheRS^Cys + Notch
Notch^RNAi

C

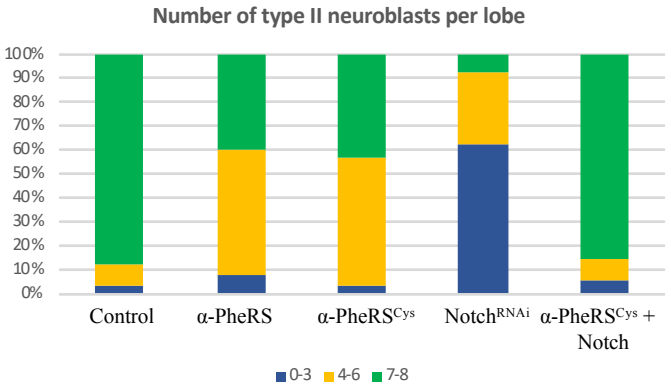
Number of type II neuroblasts per lobe
100%
90%
80%
70%
60%
50%
40%
30%
20%
10%
0%
Control
α-PheRS
α-PheRS^Cys
Notch^RNAi
α-PheRS^Cys + Notch
0-3
4-6
7-8

Figure 7

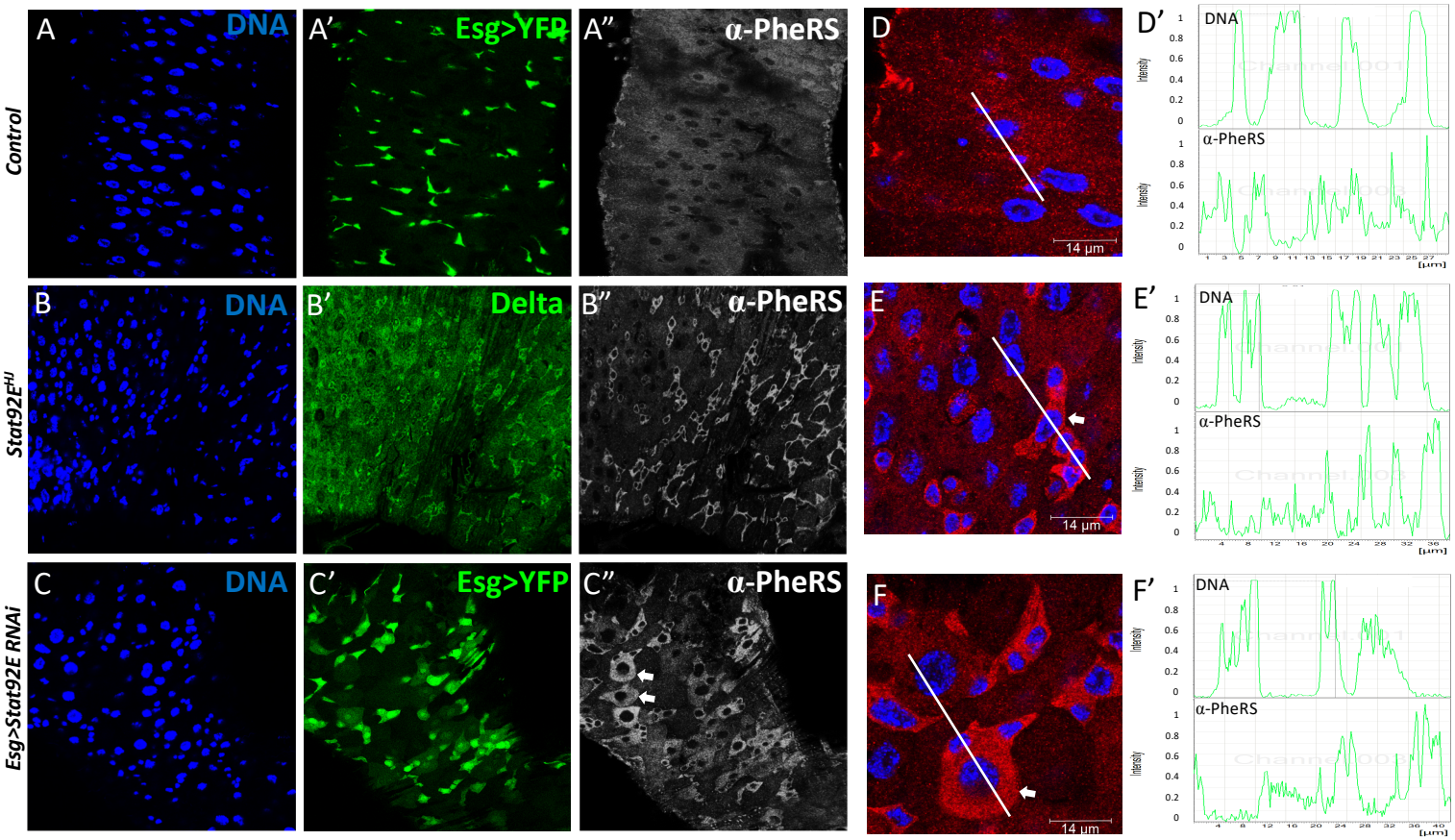
Control
Stat92E^HJ
Esg>Stat92E RNAi
A
DNA
A'
Esg>YFP
A"
α-PheRS
B
DNA
B'
Delta
B"
α-PheRS
C
DNA
C'
Esg>YFP
C"
α-PheRS
D
D'
E
E'
F
F'
14 µm
DNA
α-PheRS
Intensity

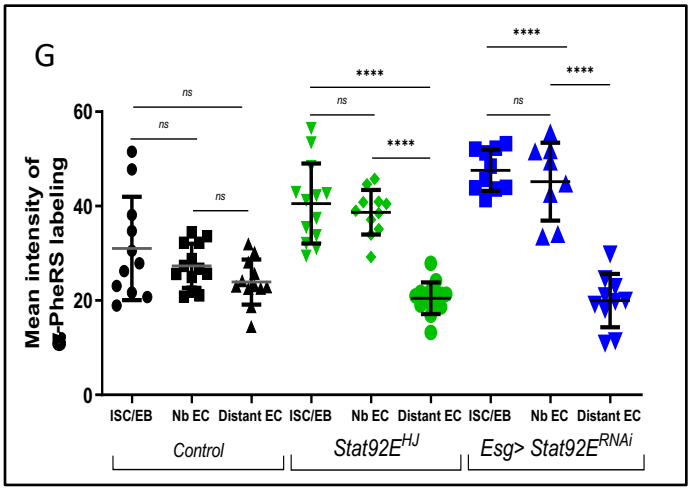
G
Mean intensity of α-PheRS labeling
60
40
20
0
ns
****
ISC/EB
Nb EC
Distant EC
Control
Stat92E^HJ
Esg> Stat92E^RNAi

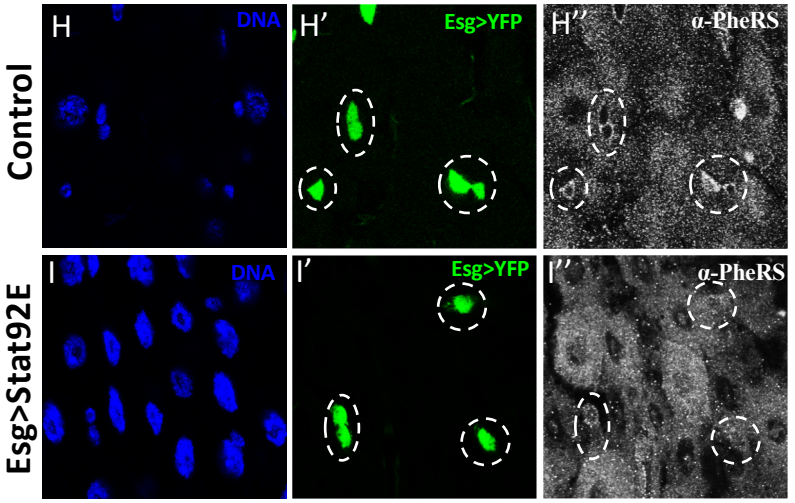
Control
Esg>Stat92E
H
DNA
H'
Esg>YFP
H"
α-PheRS
I
DNA
I'
Esg>YFP
I"
α-PheRS

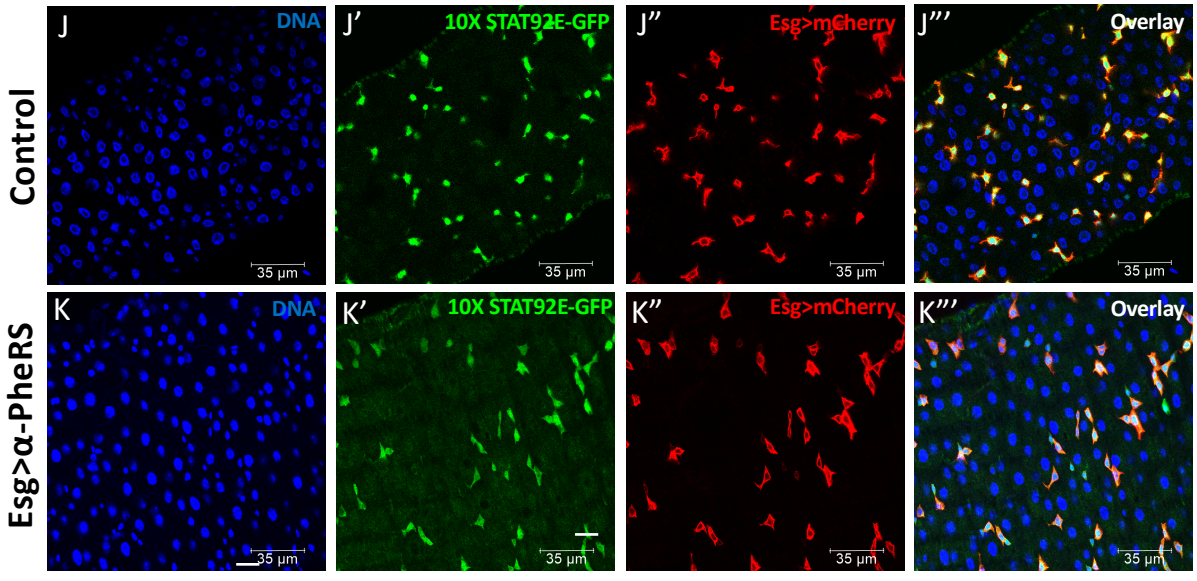
Control
Esg>α-PheRS
J
DNA
J'
10X STAT92E-GFP
J"
Esg>mCherry
J"'
Overlay
K
DNA
K'
10X STAT92E-GFP
K"
Esg>mCherry
K"'
Overlay
35 µm

Supplementary Figure S1

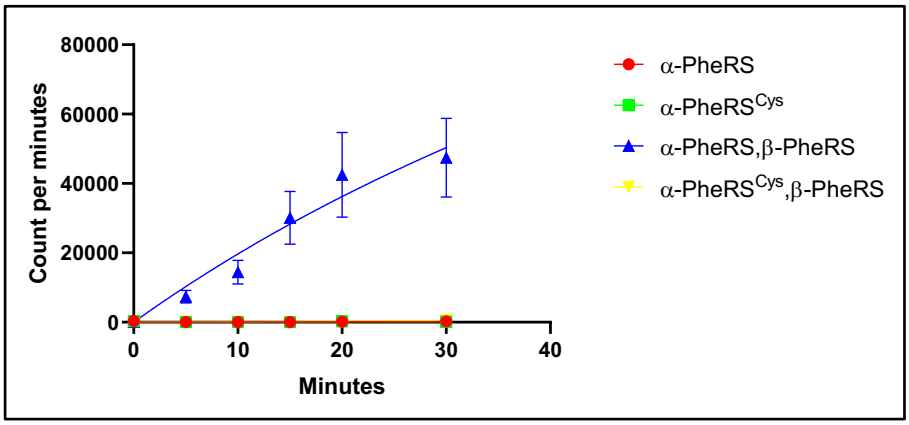

Figure S1:
The *α–PheRS^{Cys}* mutant does not support aminoacylation in vitro. The aminoacylation assay was performed with the mixture of the recombinant protein (α–PheRS or α–PheRS^{Cys} and β-PheRS) produced in E. coli. tRNA^{Phe} from yeast was aminoacylated with [^{3}H] phenylalanine. The [^{3}H] phenylalanine signal coupled with tRNA^{Phe} was counted by the scintillation counter. CPM= counts per minute.

Supplementary Figure S2

Analyzing the size of dissociated larval wing disc cells by FACS revealed that the cells from the posterior compartment (GFP-positive compartment), where both PheRS subunits were overexpressed, were on average larger than the ones that overexpressed only GFP or only α-PheRS (A). In contrast, all control cells from the anterior (GFP-negative) compartment of these three lines were of similar, smaller size (A). Cell numbers, on the other hand, did not significantly change upon overexpression of both PheRS subunits (B). We conclude that in larval wing discs with their organ size control mechanism, PheRS overexpression causes primarily an increase in cell size. On the other hand, single overexpression of α-PheRS increases the mitotic index of wing discs (Fig 1A-C).

A

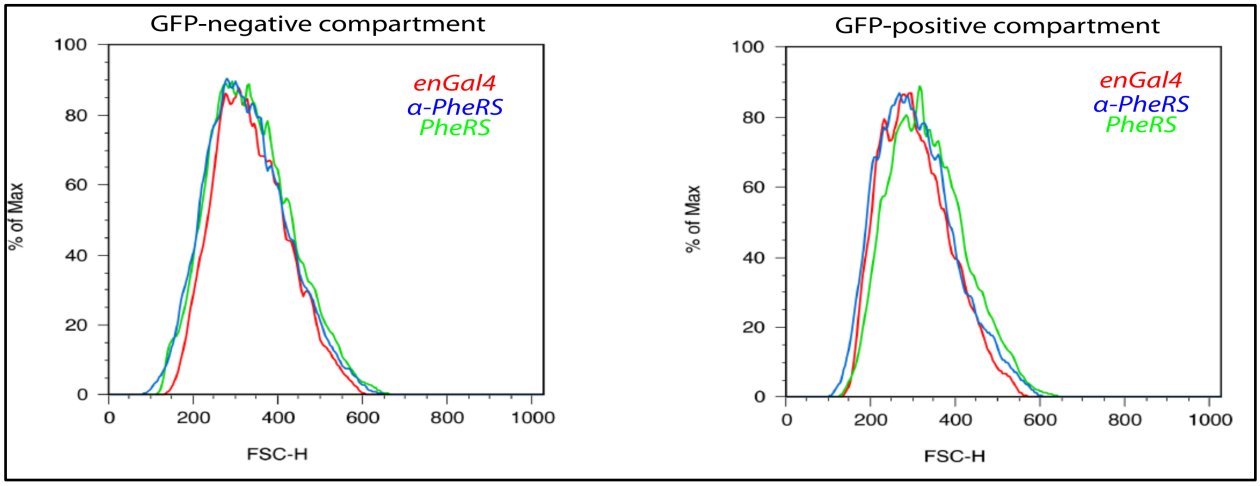

B

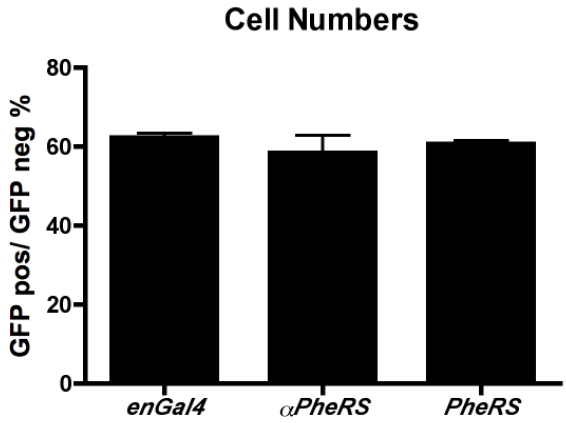

Figure S2: PheRS overexpression in wing discs increases cell size, but not cell numbers
(A) Cell size was determined by measuring the Forward Scatter (FSC) in the FACS analysis. Larvae were synchronized by using 2-hours egg lays. Late 3rd instar larvae were dissected and wing discs were dissociated. GFP was used to mark cell populations that express transgenes. The cells of the GFP-negative compartment showed similar cell size in the different lines (left panel). In the GFP positive compartment, where the transgenes were overexpressed, PheRS overexpression gave rise to bigger cells (right panel). The graph represents the results of three independent experiments. (B) Cell numbers are not significantly altered by PheRS overexpression. The experimental set up was the same as in (A). Posterior cell numbers (P; GFP positive) were determined relative to the anterior (A; GFP negative) cell numbers (n=3).

Supplementary Figure S3

Amino acid deprivation downregulates phosphorylation of dS6K in Kc cells, and subsequent stimulation with amino acids can restore this phosphorylation (Kim et al., 2008). The Rag complex is part of a nutrient sensor pathway, and its knockdown prevents the TORC1 complex from sensing the availability of amino acids (Kim et al., 2008; Sancak et al., 2008). In contrast, when *β-PheRS* was knocked down, amino acids were still able to induce phosphorylation of dS6K to similar levels as in the control. In this case, it did not matter whether all amino acids were added back (A) or only L-Phe (B). These results therefore suggest that PheRS does not serve as an amino acid sensor upstream of the TORC1 complex, although we cannot rule out that the knockdown was not sufficient to induce this effect.

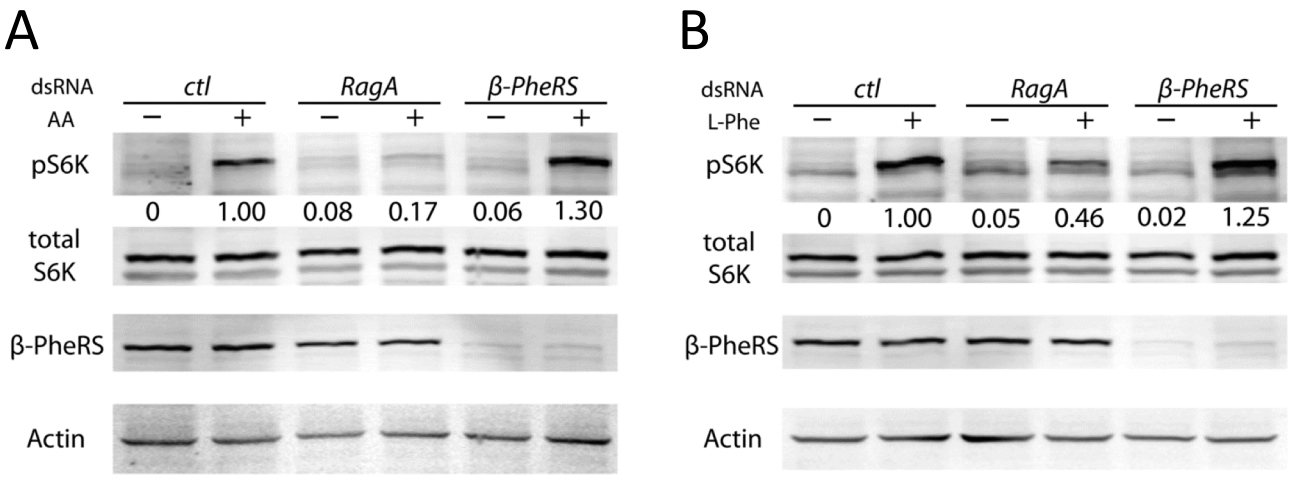

Figure S3: PheRS does not seem to serve as an amino acid sensor upstream of the TORC1 complex. (A) *β-PheRS* knockdown cannot block the TORC1 complex from sensing the availability of amino acids. Phospho-S6K was used as a readout of TORC1 signaling. Starvation (–) was performed by depriving cells from amino acids for 30 mins, and stimulation (+) was performed by adding back amino acids for 30 mins after starvation. Control is a mock RNAi *RagA* RNAi is known to block the sensing of amino acids. The level of phospho-S6K was quantified relative to the Actin level in the same extract. (B) *β-PheRS* knockdown cannot block the TORC1 complex from sensing the availability of L-Phe. The same experiment as in (A) was performed, but using L-Phe and L-Glu for stimulation. L-Glu was reported to be necessary for amino acid transport (Nicklin et al., 2009). Levels of phospho-S6K were quantified relative to the Actin levels in the same extract.

Reference

Kim, E., Goraksha-Hicks, P., Li, L., Neufeld, T.P., Guan, K.L., 2008. Regulation of TORC1 by Rag GTPases in nutrient response. Nature cell biology 10, 935-945.

Nicklin, P., Bergman, P., Zhang, B., Triantafellow, E., Wang, H., Nyfeler, B., Yang, H., Hild, M., Kung, C., Wilson, C., Myer, V.E., MacKeigan, J.P., Porter, J.A., Wang, Y.K., Cantley, L.C., Finan, P.M., Murphy, L.O., 2009. Bidirectional transport of amino acids regulates mTOR and autophagy. Cell 136, 521-534.

Sancak, Y., Peterson, T.R., Shaul, Y.D., Lindquist, R.A., Thoreen, C.C., Bar-Peled, L., Sabatini, D.M., 2008. The Rag GTPases bind raptor and mediate amino acid signaling to mTORC1. Science 320, 1496-1501.

Supplementary Figure S4

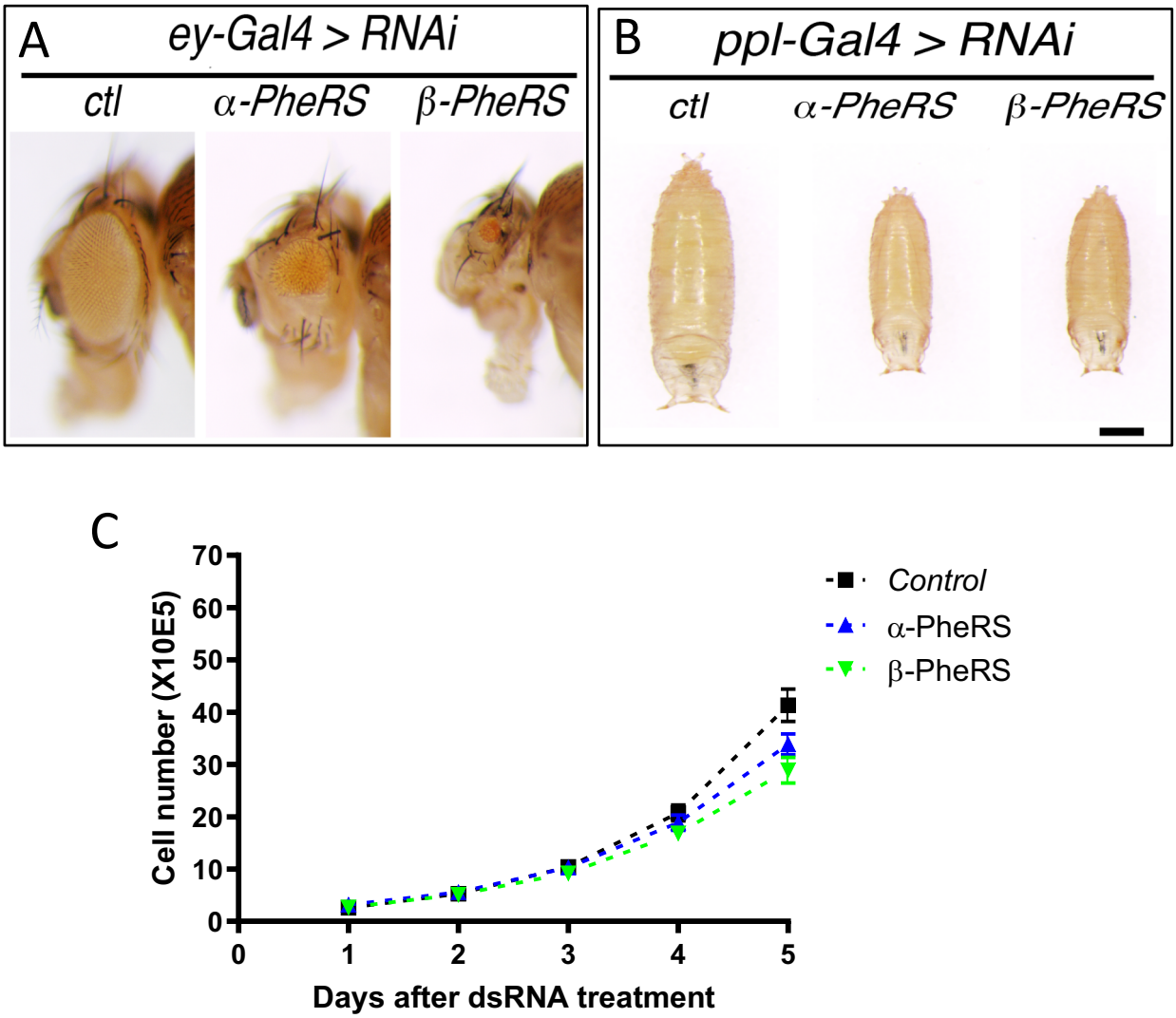

Figure S4: PheRS knockdown reduces cell proliferation and tissue size.
(A,B) RNAi knock down of *PheRS* subunits in the fly eyes (A) and fat bodies (B). *ey-Gal4* and *ppl-Gal4* were used to drive RNAi expression, respectively. The controls were GFP RNAi. RNAi knock down of either subunit reduced the eye size (A) and the size of the entire pupae, respectively. (C) Proliferation of Kc cells upon knockdown of the subunits. The control is mock RNAi. RNAi knockdown was carried out by directly adding dsRNA to the medium, and cells were harvested at days 1, 2, 3, 4, and 5 after dsRNA treatment. Knockdown of either subunit reduces cell proliferation and downregulates levels of both subunits (Lu et al., 2014).

Reference

Lu, J., Bergert, M., Walther, A., Suter, B., 2014. Double-sieving-defective aminoacyl-tRNA synthetase causes protein mistranslation and affects cellular physiology and development. Nature communications 5, 5650.

Supplementary Figure S5

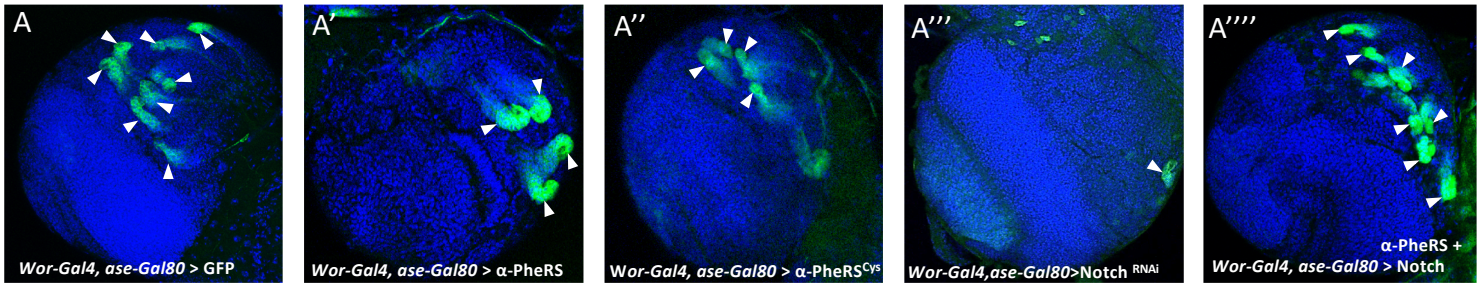

Figure S5: Overexpression of *α-PheRS* or *α-PheRS^{Cys}* in type II NBs reduced the number of type II NBs per central brain. *wor-Gal4,ase-Gal80,UAS-GFP* was used to overexpress proteins in marked (GFP signal) type II NBs. Type II NBs are pointed out with white arrowheads.